NAVAL POSTGRADUATE SCHOOL
MONTEREY, CALIFORNIA

THESIS

COMPOSITE SHIPTRACK CHARACTERISTICS

by

Raymond E. Chartier Jr.

June 1995

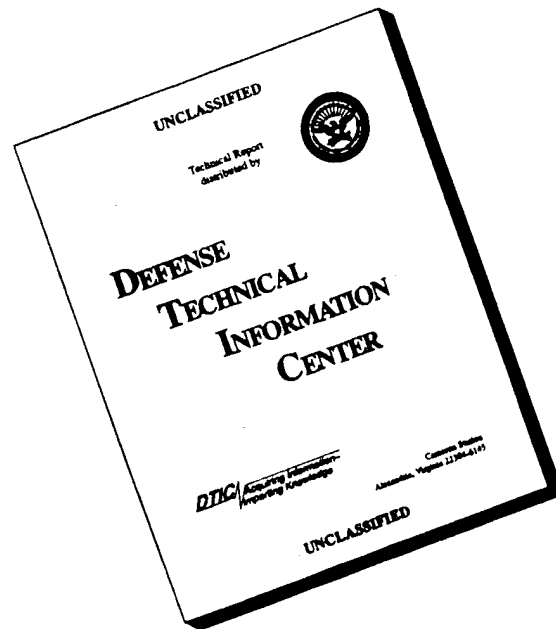Thesis Advisor: Philip A. Durkee

Approved for public release; distribution is unlimited.

DISCLAIMER NOTICE

UNCLASSIFIED

Technical Report
distributed by

DEFENSE
TECHNICAL
INFORMATION
CENTER

DTIC Acquiring Information
Imparting Knowledge

UNCLASSIFIED

THIS DOCUMENT IS BEST QUALITY AVAILABLE. THE COPY FURNISHED TO DTIC CONTAINED A SIGNIFICANT NUMBER OF PAGES WHICH DO NOT REPRODUCE LEGIBLY.

1. AGENCY USE ONLY *(Leave blank)*	2. REPORT DATE June 1995	3. REPORT TYPE AND DATES COVERED Master's Thesis

4. TITLE AND SUBTITLE COMPOSITE SHIPTRACK CHARACTERISTICS	5. FUNDING NUMBERS

6. AUTHOR(S) Raymond E. Chartier Jr.	

7. PERFORMING ORGANIZATION NAME(S) AND ADDRESS(ES) Naval Postgraduate School Monterey CA 93943-5000	8. PERFORMING ORGANIZATION REPORT NUMBER

9. SPONSORING/MONITORING AGENCY NAME(S) AND ADDRESS(ES)	10. SPONSORING/MONITORING AGENCY REPORT NUMBER

11. SUPPLEMENTARY NOTES The views expressed in this thesis are those of the author and do not reflect the official policy or position of the Department of Defense or the U.S. Government.

12a. DISTRIBUTION/AVAILABILITY STATEMENT Approved for public release; distribution is unlimited.	12b. DISTRIBUTION CODE

13. ABSTRACT *(maximum 200 words)*

Shiptracks (131) identified from Advanced Very High Resolution Radiometer (AVHRR) satellite images during the Monterey Area Shiptrack Experiment (MAST) are extracted and correlated with the ships that caused them. Composite plots and statistics of shiptrack environmental, radiative and physical properties are presented. The composite shiptrack is 296 km long, approximately 7.3 hours old, and averages 9 km wide. The head of the track has a separation distance from the ship of 16 km, and a separation time(ST) of 25 minutes. It forms in a ambient environment with a true wind of 15 kts and a low cloud reflectance in channel 3 (low 3) of 11%. The composite shiptrack has a low 3 equal to 14% and average Delta Percent Change channel 1 and 3 values of 7% and 37% respectively. Approximately 85% of the variability or "noise" in shiptracks' radiative signature is environmentally generated and occurs on the large eddy scale (1-25km). The data set was broken into subsets to isolate the effect of ship parameters on shiptrack characteristics. Variations in ship propulsion type (steam turbine verses diesel) and designed shaft power rating (kW size) produce shiptracks that are statistically different in length, width, age and reflectance. The dispersion characteristics of shiptracks were favorably compared to standard, long-range dispersion relationships.

14. SUBJECT TERMS MAST, shiptrack, composite shiptrack, dispersion, diffusion, pollution, anthropogenic aerosol, reflectivity, correlation, Gaussian dispersion model, remote sensing	15. NUMBER OF PAGES 87
	16. PRICE CODE

17. SECURITY CLASSIFICATION OF REPORT Unclassified	18. SECURITY CLASSIFICATION OF THIS PAGE Unclassified	19. SECURITY CLASSIFICATION OF ABSTRACT Unclassified	20. LIMITATION OF ABSTRACT UL

COMPOSITE SHIPTRACK CHARACTERISTICS

Raymond E. Chartier Jr.
Lieutenant, United States Navy
B.S., University of Washington, 1988

Submitted in partial fulfillment
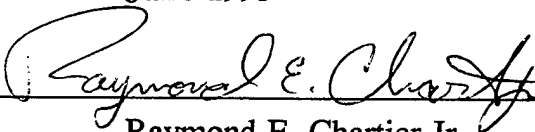of the requirements for the degree of

MASTER OF SCIENCE IN METEOROLOGY AND PHYSICAL OCEANOGRAPHY

from the
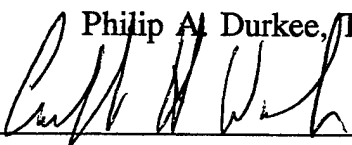
NAVAL POSTGRADUATE SCHOOL
June 1995

Author: _____
Raymond E. Chartier Jr.

Approved by: _____
Philip A. Durkee, Thesis Advisor

_____
Carlyle H. Wash, Second Reader

_____
Robert L. Haney, Chairman
Department of Meteorology

iii

ABSTRACT

Shiptracks (131) identified from Advanced Very High Resolution Radiometer (AVHRR) satellite images during the Monterey Area Shiptrack Experiment (MAST) are extracted and correlated with the ships that caused them. Composite plots and statistics of shiptrack environmental, radiative and physical properties are presented. The composite shiptrack is 296 km long, approximately 7.3 hours old, and averages 9 km wide. The head of the track has a separation distance from the ship of 16 km, and a separation time(ST) of 25 minutes. It forms in a ambient environment with a true wind of 15 kts and a low cloud reflectance in channel 3 (low 3) of 11%. The composite shiptrack has a low 3 equal to 14% and average Delta Percent Change channel 1 and 3 values of 7% and 37% respectively. Approximately 85% of the variability or "noise" in shiptracks' radiative signature is environmentally generated and occurs on the large eddy scale (1-25km). The data set was broken into subsets to isolate the effect of ship parameters on shiptrack characteristics. Variations in ship propulsion type (steam turbine verses diesel) and designed shaft power rating (kW size) produce shiptracks that are statistically different in length, width, age and reflectance. The dispersion characteristics of shiptracks were favorably compared to standard, long-range dispersion relationships.

TABLE OF CONTENTS

ACKNOWLEDGMENTS

x

I. INTRODUCTION

Shiptracks are curvilinear cloud features that are caused by ship-generated aerosols and observed in the visual and near-infrared regions of the electromagnetic spectrum. As early as 1944 there have been reports of cloud formations and alterations of existing clouds over the exhaust plume of moving vessels. For nearly thirty years shiptracks have been observed in visible satellite imagery. Their prominent appearance in near-infrared imagery has helped increase our understanding of these peculiar cloud features. Some of the more perplexing questions about shiptracks deal with their formation mechanism, necessary environmental conditions, and their long persistence. Although many questions remain unanswered, there are two undisputable facts that provide the starting point for this thesis research. First, shiptracks indicate a localized perturbation or alteration to the cloud microphysical structure which changes the radiance signature as compared to the unaffected, ambient cloud. Secondly, shiptracks conveniently act as giant curvilinear "pointers". The tip, or shiptrack head, points to the location of the ship that is responsible for its formation. The potential for shiptrack use in intelligence and surveillance application is clearly evident.

The science and environmental applications are also significant. Some of the research areas that will benefit from a more complete understanding of shiptracks are: remote sensing (interpretation, application), cloud microphysics and long-range pollution transport and dispersion. The effect of anthropogenic aerosols on climate has received considerable international attention (IPCC, 1994). A more complete knowledge about shiptracks will help quantify the process by which aerosols (specifically anthropogenic) increase cloud reflectance (albedo), decrease solar heating and force local and global climate response (Albrecht, 1989; Charlson et al., 1987; Charlson et al., 1992).

To this end a comprehensive multi-platform, inter-disciplinary science experiment was conducted off the coast of California during the month of June 1994. The primary objective of the Monterey Area Shiptrack Experiment (MAST) was to determine the ship-related necessary conditions for the formation of surface ship cloud effects in a region and at a time known to support formation of these effects (ONR, 1994).

1

Prior to MAST only 27 direct correlations had been made between shiptracks and ships responsible for their formation. As a result, most shiptrack studies dealt with individual shiptracks or a small number of shiptracks in a case study approach. The problem unresolved in those studies was that the radiative signature of a single shiptrack is quite "noisy" (high variability), therefore the "signal" or trend can be obscured or undeterminable. A composite technique, utilizing statistics and filters, is used here to reduce the signal to noise ratio in the shiptrack data series.

This thesis uses the MAST data set with emphasis on the satellite-retrieved radiance signature of a statistically significant set of 131 ship to shiptrack correlations. These data is used to accomplish three goals: 1) describe and quantify nominal shiptrack characteristics and use this information to determine if ship specific characteristics (e.g., propulsion type, power rating, etc) can be ascertained from shiptrack radiative properties. 2) quantify the radiative effects of anthropogenic aerosols in marine stratus clouds 3) test relevant MAST hypotheses through the use of composite shiptrack characteristics and statistics.

Chapter II provides some background and theory pertaining to shiptracks and diffusion parameters used. Chapter III explains how the data set was formed, correlations were made and other procedures of significance. The results are presented in Chapter IV including composite shiptrack plots and statistics. This section lists the composite shiptrack characteristics (the "signal") and reports the cause(s) of the noise inherent in the data. Modified Gaussian dispersion model results is also presented. Chapter V contains conclusions and recommendations for future research.

II. BACKGROUND AND THEORY

A.   SHIPTRACK BASICS

The National Oceanic and Atmospheric Administration (NOAA) polar orbiting satellites are one of the best platforms to observe ship-aerosol effects on clouds. They are equipped with the Advanced Very High Resolution Radiometer (AVHRR) which has five channels and a resolution of 1.1 km by 1.1 km at nadir. Channel 1, centered at .63 μm and channel 3, centered at 3.7 μm, are very useful in shiptrack analysis. Figure 1 shows a comparison of shiptracks as seen by visible and near-infrared wavelengths. Notice the increased number and clarity of shiptracks in the 3.7 μm image. The reason is cloud reflectance in visible wavelengths is dependent upon droplet size, liquid water content and cloud thickness while cloud reflectance at 3.7 μm is determined by water droplet radius alone (in an inverse relationship) assuming cloud thickness is greater than 100 meters. In-situ aircraft measurements of shiptracks indicate that stack emissions from a ship passing under stable stratoform clouds serve as a source of cloud condensation nuclei (CCN) which increase the number of water droplets and reduce the average droplet size resulting in a detectable increase in 3.7μm radiance (Radke et al., 1989; King, 1990). Figure 2 illustrates this process and graphically shows the advantages of using channel 3 to study shiptracks. A more through discussion on the effects of aerosol particles on cloud radiative properties can be found in Mineart (1988).

Figure 2 also illustrates the proposed shiptrack formation mechanisms. Ship-exhaust adds gases, heat, moisture and combustion particles to the environment. The gases (after a gas to particle conversion process) and combustion particles serve as CCN sources. Buoyancy from exhaust heat and increased vertical motion due to ship-induced mechanical turbulence may enhance near-ship boundary layer mixing and shiptrack development (Hindman, 1990; Porch, et al., 1990). A near-neutral marine atmospheric boundary layer (MABL) has a typical mixing time of 20 to 30 minutes.

3

Figure 1. Comparison of AVHRR Ch. 1 (0.6μm) (left) and Ch. 3 (3.7μm) (right) for 27JUN87 2247UTC.
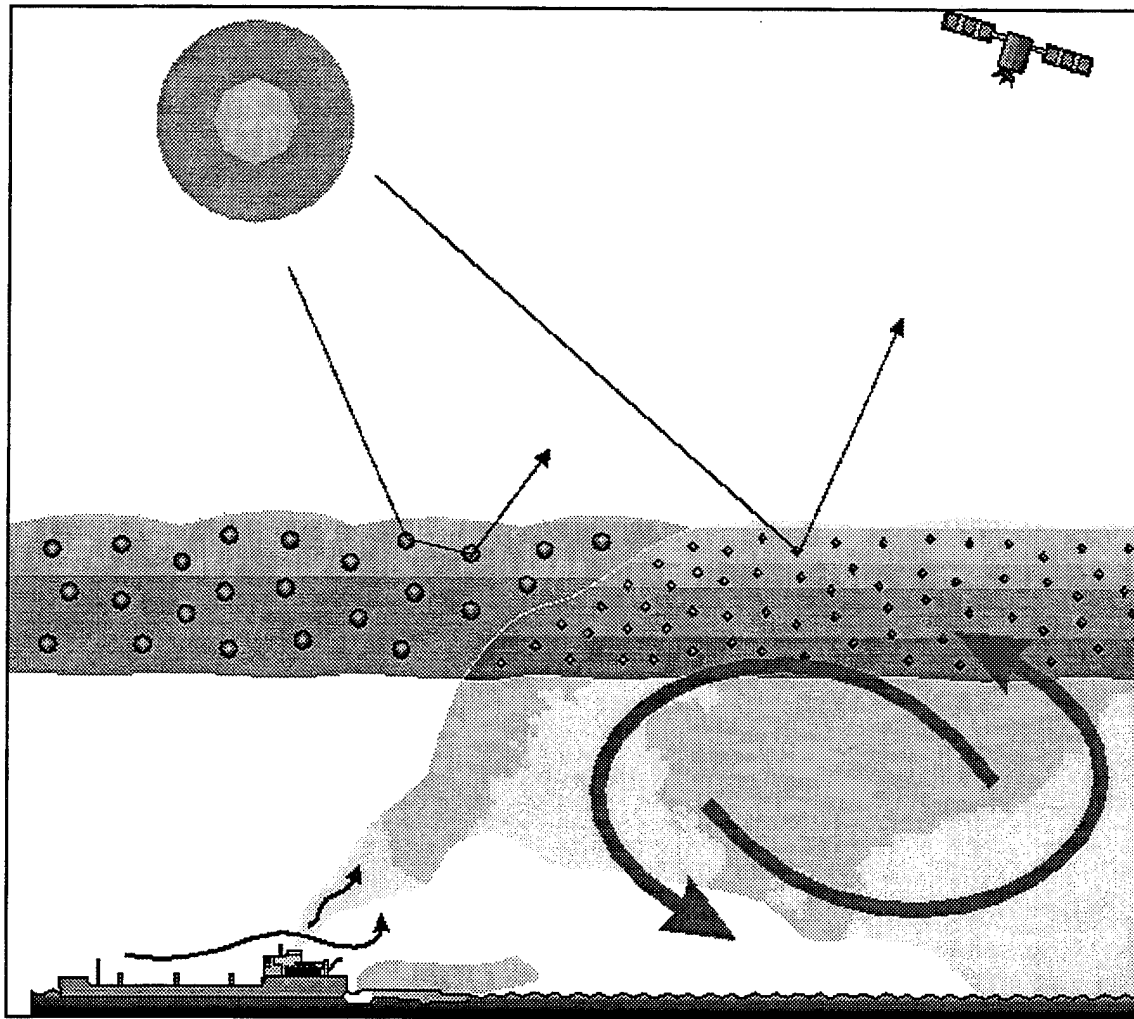
Figure 2. Shiptrack Formation Mechanisms. Aerosol produced by ship stack and ship wake are introduced into the Marine Atmospheric Boundary Layer (MABL). Large, curved arrows represent turbulent mixing in the MABL. Thin, curved arrows represent buoyancy due to exhaust heat and mechanical turbulence due to ship's motion through the MABL. Thin, linear arrows represent solar radiation at 3.7µm. Increased reflection of solar radiation at this wavelength from ship-influenced cloud is due to greater scattering by smaller radius water droplets formed by ship-produced aerosol. Lower reflection from uncontaminated cloud is due to greater absorption by larger radius water droplets at 3.7µm. After Brown (1995).

5

Figure 2 indicates that there is a finite distance between where the ship emits exhaust and where its effects are first observed remotely. Rogerson (1995) conducted a detailed analysis on 99 correlated shiptracks. He found that the separation time (ST) associated with this distance, is 24.7 minutes on average. This suggests that normal MABL mixing predominantly drives the initial shiptrack formation process.

The persistence of shiptracks is intriguing. They remain intact and distinct in satellite images for hundreds of kilometers downwind of the responsible ships. The same shiptrack can remain detectable for one to two days and typically have widths of 8-12 km. What determines shiptrack persistence is not fully understood. Most likely normal diffusion of ship-aerosols by mesoscale and synoptic scale turbulence is responsible. Porch et. al,. (1990) gave physical evidence for the strong influence of diffusion processes on shiptracks when they reported that a ship moving at 9 m/s produced shiptracks with widths that widen to 3-6 km over 40 km; which are consistent for non-shiptrack plume widths from stationary sources listed by Gifford, (1985). A second possibility is the persistence is forced by radiative-induced circulations in the area of the shiptrack (Durkee, 1994).

The frequency of shiptrack occurrence is driven by two factors; the ship characteristics and background environmental conditions. A ship must be capable of supplying enough aerosol to produce a noticeable microphysical effect i.e., a threshold aerosol concentration must be exceeded before a shiptrack can be observed with 3.7 μm observations. For example a 30 m long ship with a small total maximum designed shaft power (hereafter referred to as power rating) of 3000 kW is far less likely to make a shiptrack than a 200 m long container vessel with a power rating of 20,000 kW. The threshold value is not currently known nor is it likely to be a constant. It is highly dependent upon the background aerosol concentrations and other environmental factors. Without a doubt, the most critical factor dictating shiptrack formation is the environment.

B.   BACKGROUND ENVIRONMENTAL CONDITIONS

Conover (1966) suggested several ambient conditions necessary in the marine atmosphere before shiptracks will form. They are: 1) a shallow, cloud-topped, well-mixed boundary layer; 2) a low number of CCN; and 3) a relatively narrow range of temperatures and relative humidities at the surface. Trehubenko (1994) reported the MAST specific composite shiptrack environment to be in close agreement with Conover's conditions. Specifically, some of the mean values observed were: boundary layer depth (BLD) 504 ± 125 m, air temperature minus sea surface temperature -0.3 ± 0.8 °C, relative humidity 89.7 ± 6.5, surface pressure of 1018.3 ± 2.4 mb and true wind speed of 7.8 ± 3.0 m/s. For a synoptic weather summary for MAST the interested reader is referred to Brenner (1994). Brenner also addresses the low CCN concentration "clean" stratus versus high ambient CCN (from continental sources) or "dirty" stratus environments and their effects on reflectivity. He showed that continentally affected stratus has a very bright appearance. Thus shiptracks are less likely to be observed in dirty stratus regions due to the elevated ambient brightness.

C.   WHY THE COMPOSITE APPROACH?

As stated above, a single shiptrack displays a high degree of scatter or variability in its radiative signature. Figure 3 shows the large variability in the fractional change in channel 3 reflectance [Delta Percent Change (DPC 3)] values with distance downtrack [X(km)] for the breakbulk cargo carrier Star Livorno at 0052UTC on 30JUN94.

Mathematically DPC 3 is

$$DPC\ 3 = \frac{low3_{st} - low3_a}{low3_a} \, 100\% \ ,$$

where low 3_{st} is the low 3 reflectance of the shiptrack and low3_a is the low 3 reflectance of the ambient cloud. Stated simply, DPC values quantitatively show how different a shiptrack is from its ambient environment.
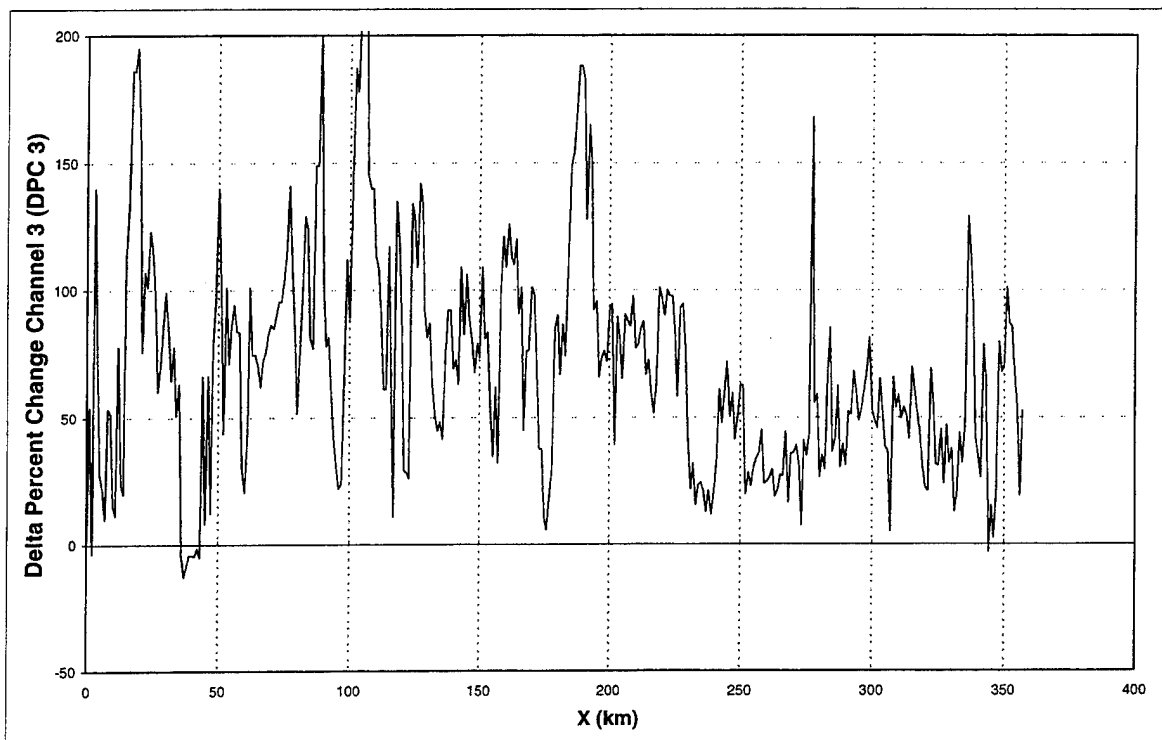
Figure 3. Example of variability or "noise" in the DPC 3 verses distance downtrack (X) for a ship, Star Livorno (S6BO) on 30JUN94 at 0052 UTC.

All shiptracks have a comparable amount of variability in their radiative signature. The variability occurs predominantly on a small scale (1-25 km) is due to stratus irregularities and brokenness, cirrus cloud interference, cloud roll structure, large eddy size variations and crossings with other shiptracks. It strongly masks a shiptrack's radiative signature. To remove this "noise" the composite approach was employed. The variability in one shiptrack signature should not be correlated to the variability in other shiptrack (i.e., the variability is random). Thus the composite of many shiptracks will average out the variability in any single shiptrack. The result is a composite shiptrack, from which trends of radiative and physical characteristics can be determined.

D. DIFFUSION AND DISPERSION

Pollution studies have historically modeled emissions from a continuous point source as a conical plume with a Gaussian distribution as is shown in Figure 4a. The conducive shiptrack environment mentioned above produces a boundary layer with near-neutral stability capped by a subsidence inversion aloft. Ship exhaust released in this type of marine boundary layer results in a trapped plume as shown in Figure 4b. When neutral atmospheric conditions exist, plumes are diffused by mechanical turbulence. The turbulence intensity is a function of sea surface roughness, height in the MABL, and most importantly, wind speed. This type of plume is especially suited to be modeled by the Gaussian diffusion equation because a major part of the pollutant concentration is carried significantly downwind before reaching ground level in significant amounts (Wark and Warner, 1976).

9
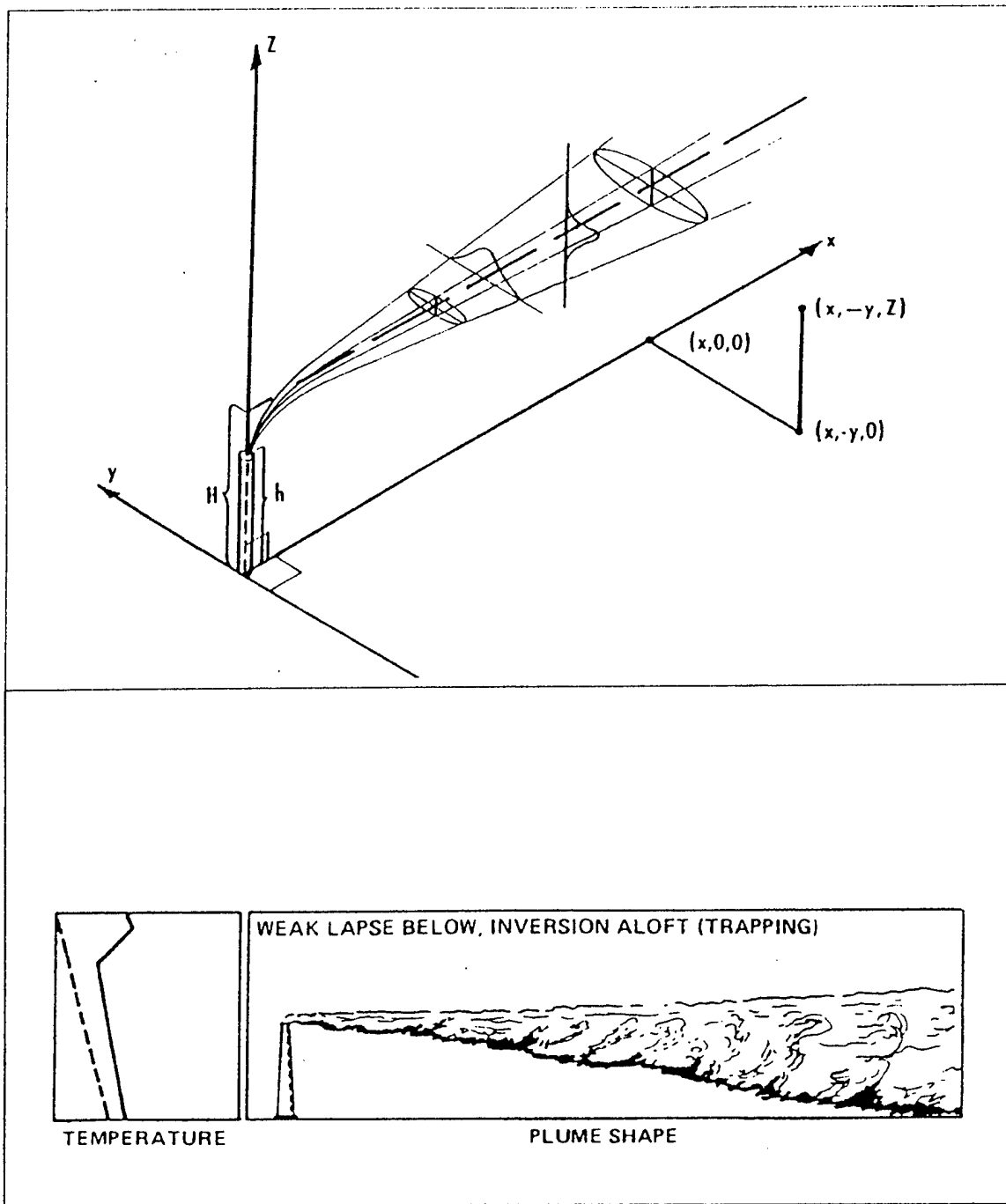
Figure 4. (a) Idealized conical plume with a Gaussian distribution. Often used to model emissions from a continuous point source. From Turner (1994). (b) Sketch of a trapped plume in a boundary layer with near neutral stability capped by a subsidence inversion. From Zannetti (1990).

The "far field" form of the Gaussian plume model for a fixed continuous source in a well-mixed boundary layer is

$$C(x,y) = \frac{Q}{\sqrt{2\pi}\,UH\sigma_y}\, e^{-\frac{y^2}{2\sigma_y^2}}$$

where C is concentration (gm^{-3}), Q is source strength (gs^{-1}), U mean wind speed (ms^{-1}), H mixed layer depth (m), σ_y is the horizontal plume dimension (m), (also known as the standard deviation of the concentration distribution at the downwind distance X), and x, y are the downwind and crosswind coordinates.

Long-range (greater than 10 km) diffusion and transport models over *land* are available. However, there is no definitive one because there are simply too many missing pieces of information, such as σ_y or K_y (diffusivity) coefficients at these scales. To the author's knowledge no long-range diffusion model exists for over water, especially not one that is based on actual field experiments extending over the ranges that shiptracks are observed. Skupniewicz (1995) developed an estimation of shiptrack horizontal plume dispersion parameters (σ_y) based on the "opacity method" introduced by Roberts (1923) and applied to dispersion studies by Gifford (1957, 1959, 1980). σ_y is estimated directly from the observed brightness patterns of shiptracks. It is independent of the source characteristics and cloud microphysics. Figure 5 shows an idealized plume shape as seen from above, the equation for σ_y and the relationship between the instantaneous standard deviation (σ_y) and the observed width of the plume (y_e). At the position of maximum visible width $\sigma_y = y_e = y_e$ max. For a more rigorous explanation of the adaptation of the opacity method to shiptrack analysis, see Appendix A by Skupniewicz (1995).
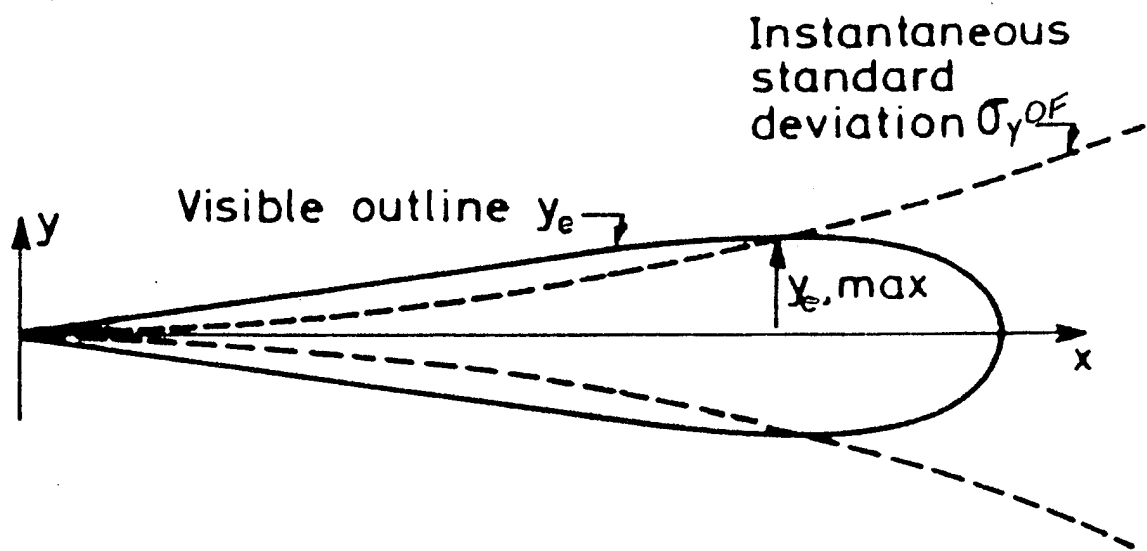
Figure 5. Idealized plume shape as seen from above. After Mikkelsen (1983). The equation for σ_y is, $\sigma_y^2(x) = y_e^2 [\ln (e\rho^2) - \ln \sigma_y^2(x)]^{-1}$. For more detail see Appendix A.

This thesis uses this new approach in two ways, first as an additional parameter for composite shiptrack analysis, and secondly as an independent variable in a ship power rating prediction model.

E.   MAST HYPOTHESES

To meet the objectives of the MAST experiment, a number of hypotheses were tested. In general they addressed: aerosol/cloud interactions and detailed microphysics; boundary layer perturbations by ships; cloud dynamics; and background environmental conditions (Durkee, 1994).

Hypotheses pertinent to this thesis are:

1. Submicron aerosol particles from the ship stack are responsible for cloud droplet and radiative features of ship tracks.

2. Gas-to-particle conversion provides a source of CCN for cloud modification downtrack.

3. Heat and moisture injection from ship stack enhances buoyancy and vertical motion affecting (a) cloud formation and (b) the delivery of aerosol to the cloud base.

The composite technique results presented in this thesis quantifies attributes and peculiarities of many shiptracks. The composite shiptrack contains information about the microphysical changes (hypothesis 1), and formations mechanisms (hypotheses 2,3) that caused and sustain it.

III. DATA AND PROCEDURES

A. DATA

1. Shiptracks

Shiptracks and shiptrack heads were visually identified, and cataloged from NOAA 9/10/11/12 AVHRR satellite imagery collected during the MAST experiment. Up to 10 passes per day were obtained from these polar orbiting platforms and the greatest gap in coverage was between four to six hours. Figure 6 shows the geographical locations of the 1362 shiptrack heads identified during the month of the experiment. As might be expected, a heavy concentration of head points lie along the great-circle shipping lanes. Additionally, 735 shiptracks were individually extracted (process explained later) using the shiptrack extraction algorithm developed at NPS by Nielsen and Durkee (1992). Not every shiptrack head resulted in a shiptrack extraction. Often shiptrack heads are distinct but the rest of the track is faint or otherwise inadequate to warrant the effort required to extract it. Figure 7 shows the extracted track for the container ship Sea-Land Consumer (callsign WCHF), and a zoomed portion of the NOAA image from which it was derived. Appendix B tabulates shiptrack frequency of occurrence data for the month of June.

2. Ship Position Data

Accurate ship position data were used to make correlations between shiptracks and the ship that formed it. The ship position data were acquired from three sources. Fleet Numerical Meteorology and Oceanography Center (FNMOC) provided positions of ships on the ship synoptic weather reporting system. The ships report their international call sign, position, various weather parameters (including the true wind (Ut)) and the date-time-group (DTG). The bulk of the reports are at synoptic weather reporting times (0000, 0600, 1200, 1800 Universal Time Coordinated (UTC). These reports provided 7693 ship and buoy positions during the MAST experiment.

The second source was the Joint Maritime Information Element (JMIE) Support System (JSS). It provided 10,788 ship position reports. The JSS is a U.S. Coast Guard (USCG) maintained database and consists of multi-source, world-wide, maritime-related
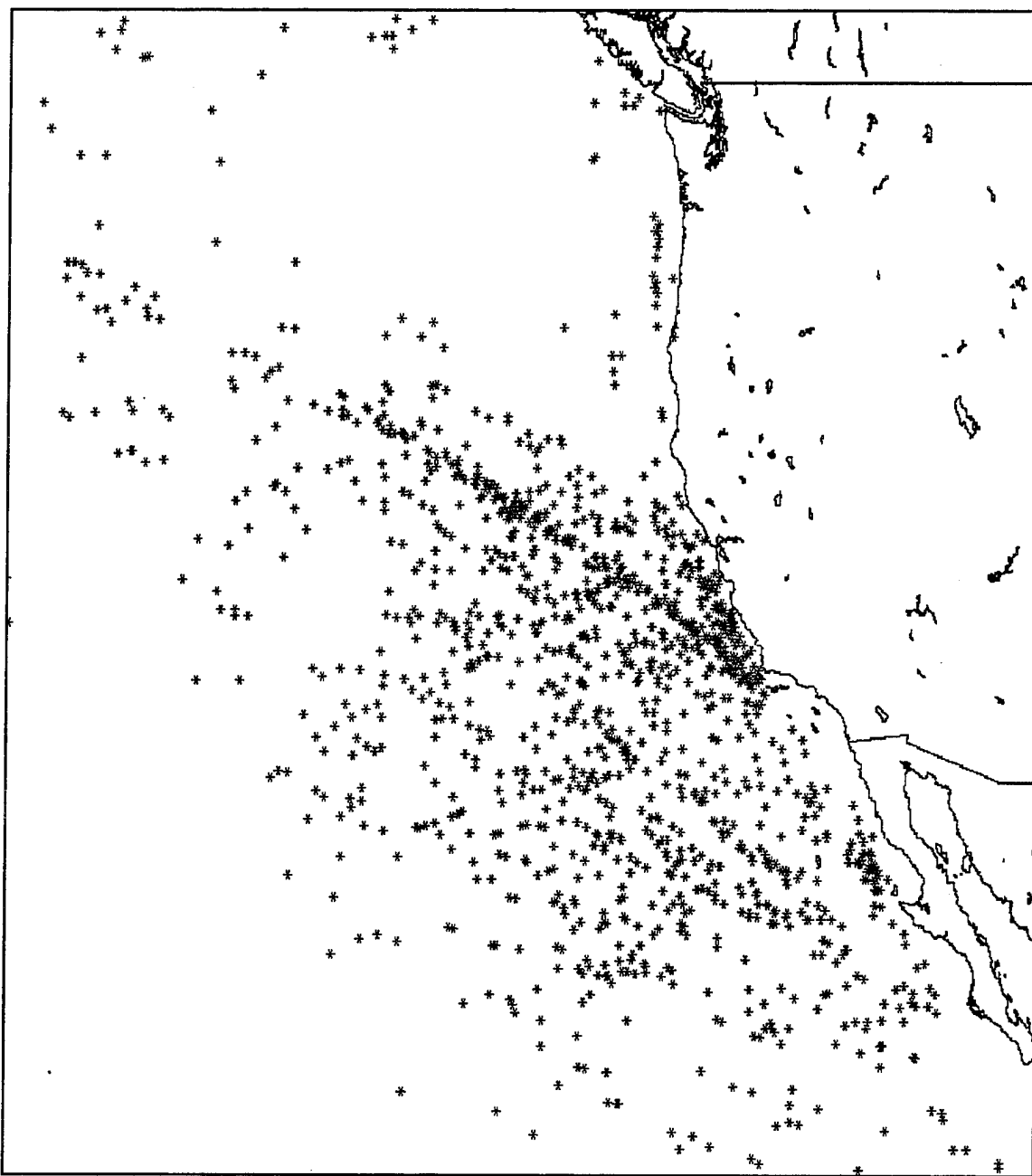
Figure 6. Shiptrack Head Points (1362) from MAST Experiment of June 1994 identified from NOAA 9/10/11/12 AVHRR Channel 3 (3.7μm) imagery.
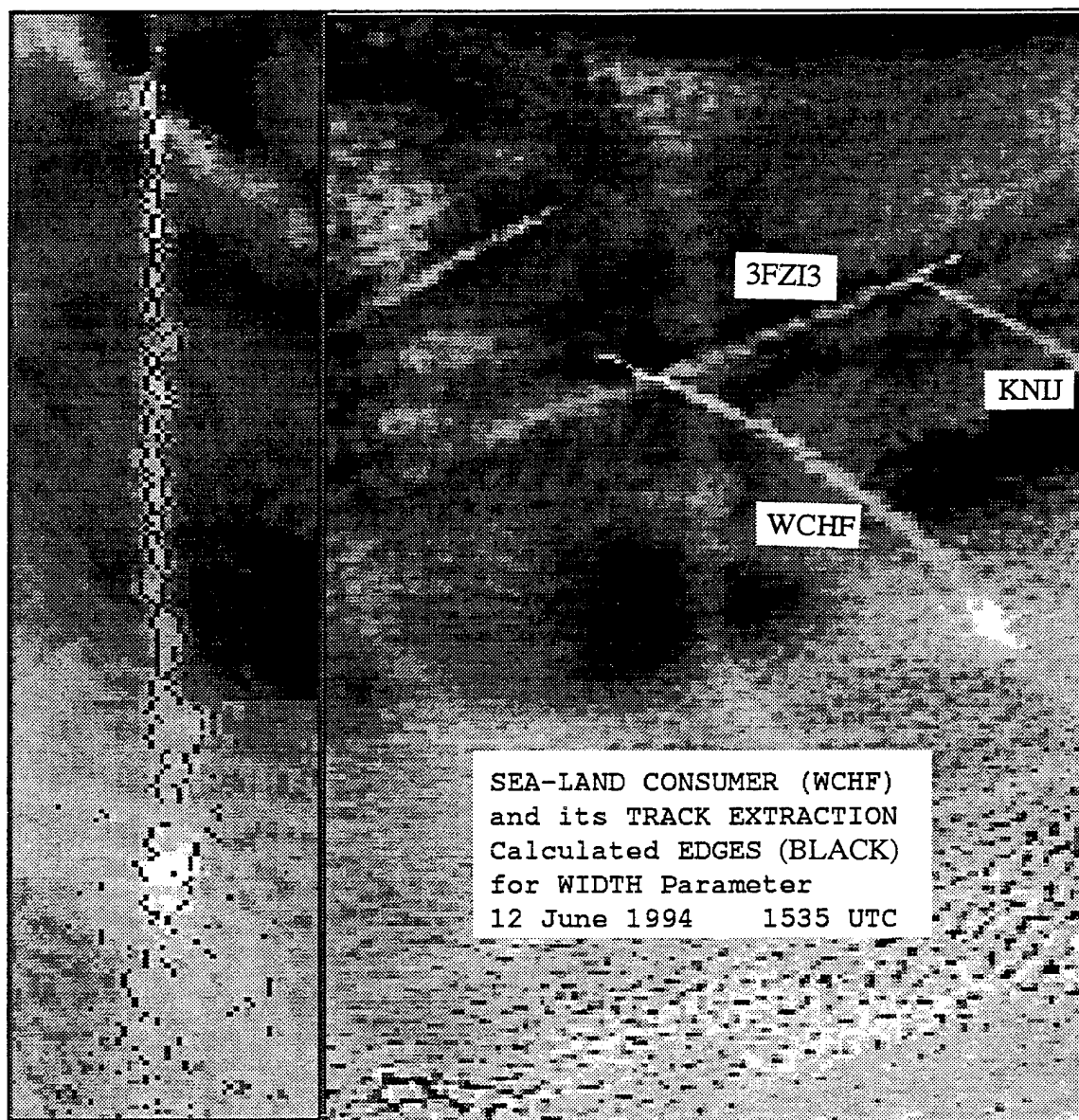
Figure 7. (a) (right pannel): Zoomed NOAA Image on 12JUN94 at 1535Z showing the shiptracks of the vessels Sea-Land Consumer (WCHF), Manulani (KNIJ), and Scarlet Success (3FZI3). The distances from the headpoint of KNIJ to the heads of WCHF and 3FZI3 are 135km and 35km, respectively. WCHF and KNIJ have identical ship characteristics (propulsion, type of vessel, size, power rating, etc.) and have identical course and speeds. (b) (left pannel): WCHF's extracted shiptrack. Dark pixels on plume edges mark the width of the shiptrack as defined by the extraction algorithm.

data, pooled into one central database. These data included off-synoptic time reports as well most of the FNMOC reports. Thus many of the gaps in the FNMOC data were filled by JSS data. Figure 8 depicts the graphical distribution of all 10,806 ship reports used to make correlations.

MAST research aircraft also provided some ship position reports, albeit limited in number. Some of these reports were essential to make correlations near land where ships are less likely to report due to navigational and operational considerations.

3. Correlations

A correlation consists of an identified shiptrack and the name and position of the ship that formed it. For a correlation to be made the ship and the shiptrack must pass three criteria. They must be collocated in space and at the same time. The last criteria is one of orientation. The youngest portion of the shiptrack must be oriented in the direction of the relative wind for that ship. The oldest portion of the shiptrack must display an appearance in agreement with the true wind field pattern. In other words, a west-bound ship with northerly winds has a relative wind from the northwest and a shiptrack that extends southeast of the ships position. For a detailed explanation of the correlation technique developed by this author and Brown, see pages 9-15 of Brown (1995).

From the MAST data set 209 correlations have been made thus far. Figure 9 shows the head point location for 209 correlations. Only 131 correlations were used in the composites. Attrition was due to the removal of night correlations and correlations with incomplete image and/or ship (position, characteristic) data. Figure 10 lists some of the information that was gathered for each of the 209 correlations. It contains a picture of the Hanjin Barcelona, some of her pertinent ship characteristics and some correlation information. Appendix C lists the ship characteristics obtained for all correlated ships. Those correlations used in this study are indicated (*). Appendix B tabulates correlation data for the month of June 1994. Approximately 28% of all extracted shiptracks were correlated to the ship that produced it. Table 1 lists a brief summary of correlation data from Appendix C. The value in parenthesis is the number used for this study.

18
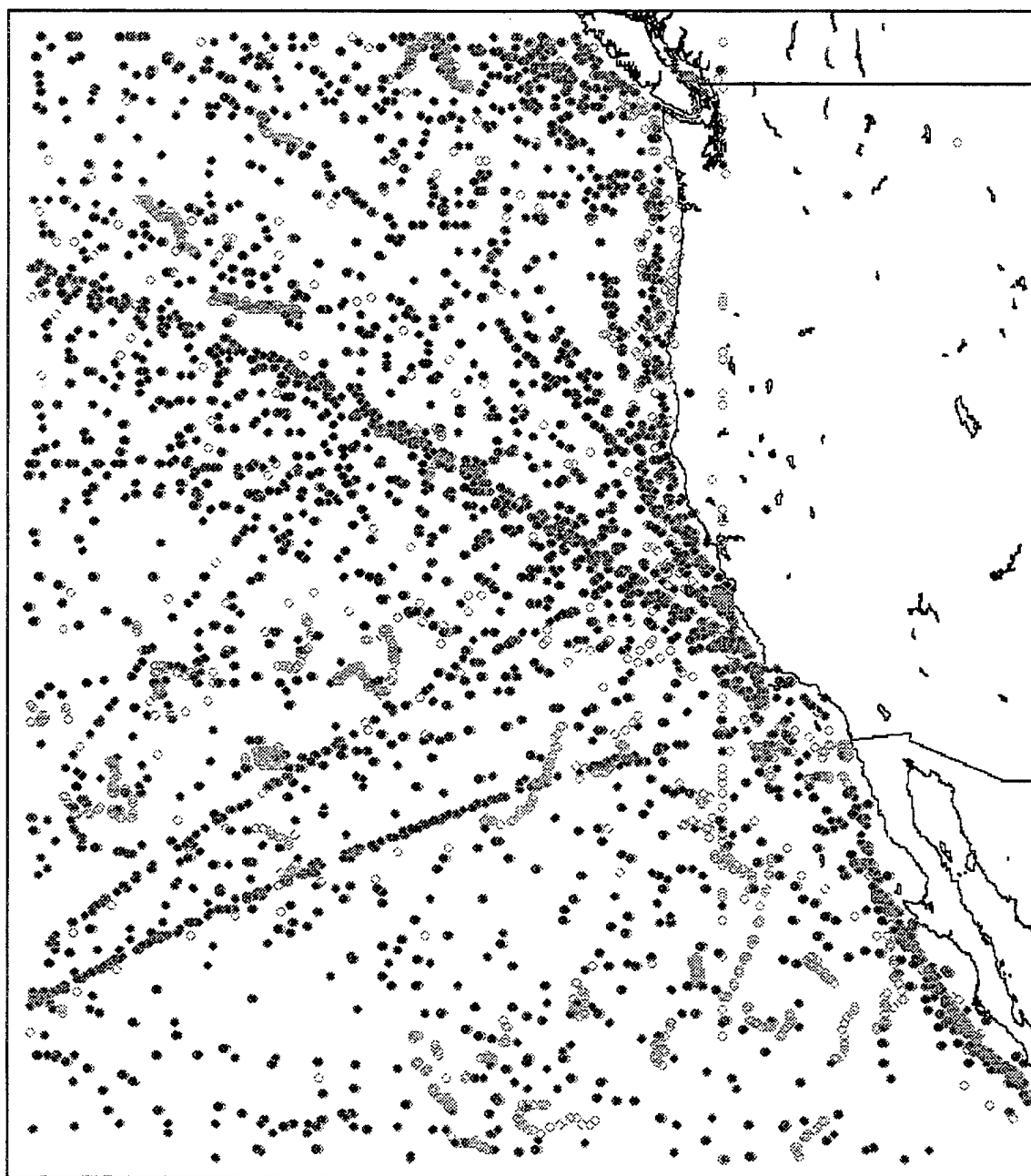
Figure 8. Ship Reports (10,806) from FNMOC (circles) and JSS (dots) databases for June 1994. Note that most of the FNMOC Reports are contained within the JSS database.
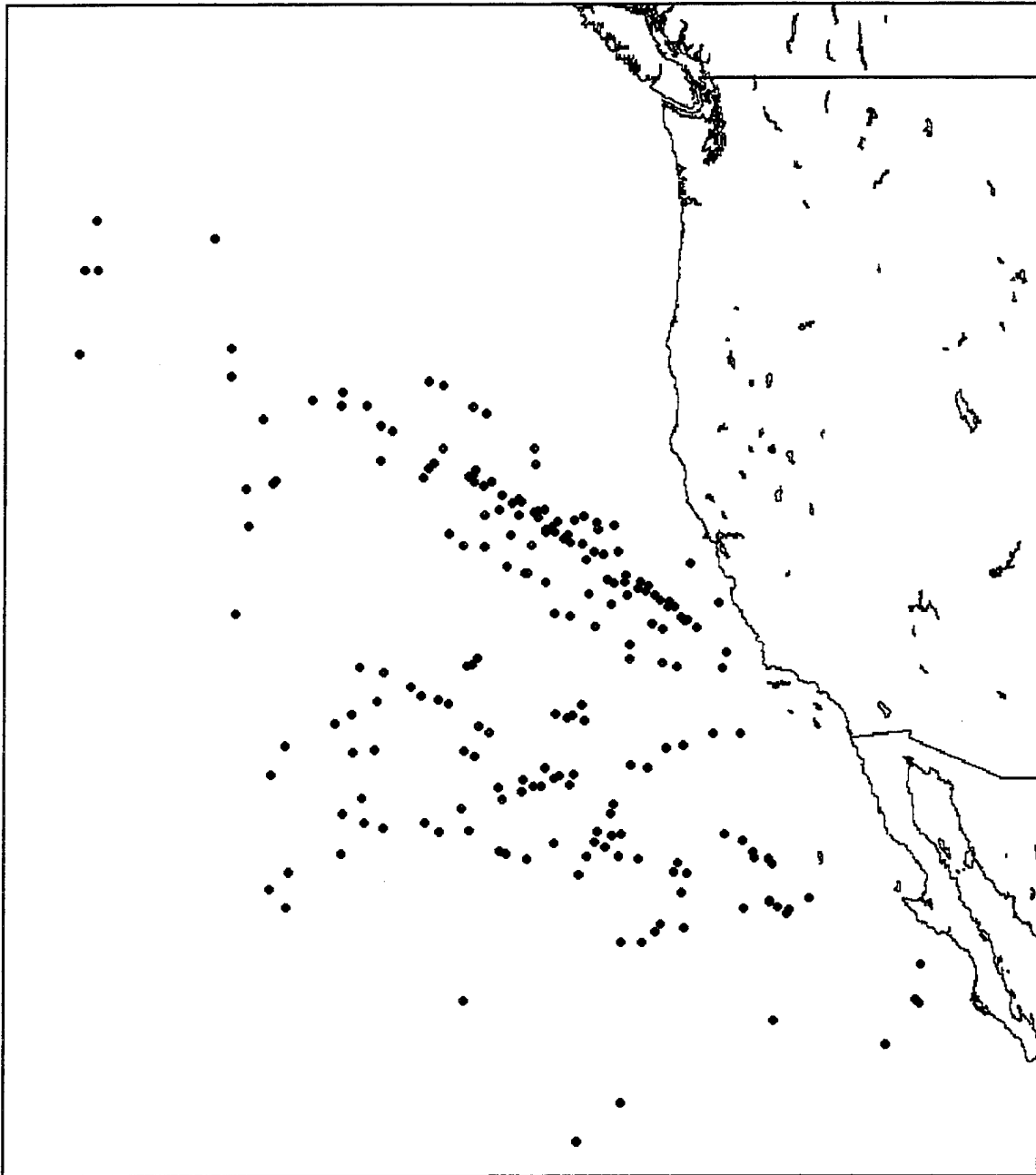
Figure 9. Correlations (209) made between shiptracks from MAST and ship reports from FNMOC and JSS databases.
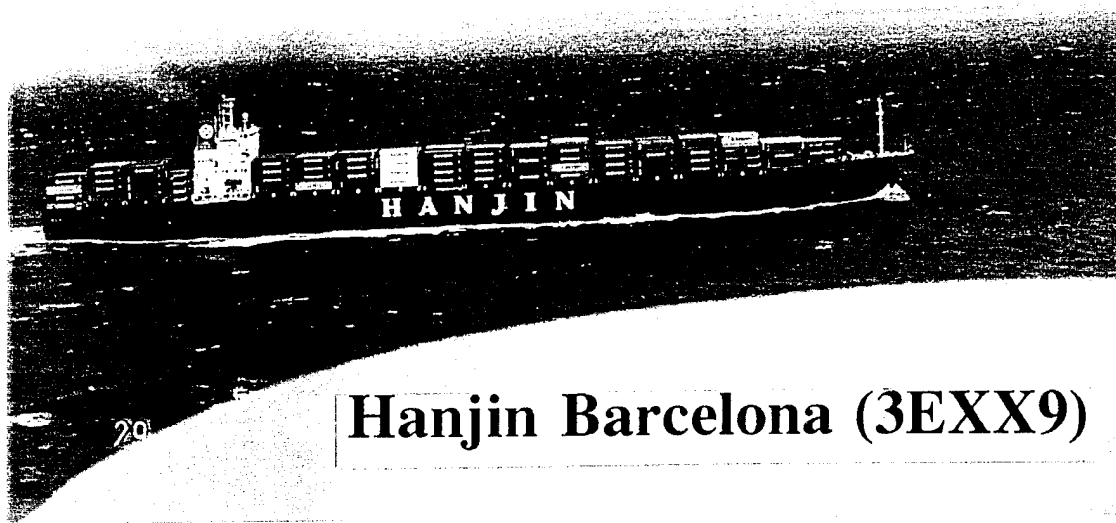
Hanjin Barcelona (3EXX9)

TYPE	CONTAINER SHIP
GROSS TONNAGE	50,792
PROPULSION TYPE	DIESEL
FUEL TYPE	H.V.F., D.O.
POWER RATING	52,236 bhp = 37,868 kW
LENGTH	289.5 meters
COURSE/SPEED	120/23 kts
# OF CORRELATIONS	FIVE, 14 hrs 29-30JUN94
TRUE WIND	350/18 kts
RELATIVE WIND	070/18 kts

Figure 10. Picture and Summary of Correlation and Ship Characteristics for the Hanjin Barcelona. (H.V.F. stands for high viscosity fuel, D.O. stands for Diesel oil.).

21

Propulsion Type	No. of different ships	No. of correlations
Steam Turbine	13 (8)	33 (17)
Diesel Engine	61 (44)	176 (114)
Totals	74 (52)	209 (131)

Table 1. Summary of Correlation Statistics for MAST.

B. PROCEDURES

1. Satellite Retrieval Technique

The retrieval process begins with conversion of AVHRR sensor raw count values to engineering units. Channel 1 and 2 units are converted to percent albedo while channels 3, 4, 5 are presented in brightness temperatures based on a linear calibration relationship, and an inverse Planck function. To get cloud reflectance, an anisotropic reflectance factor (ARF) is used to correct for the specific angular geometry between sun, reflecting surface, and satellite for each pixel. AVHRR products utilized in this study are:

1. 'low 1' - low cloud reflectance; channel 1 ARF applied

2. 'low 3' - low cloud reflectance; channel 3 ARF applied

3. 'ch4' - cloud temperature; channel 4

Brenner(1994) provides more detail on the retrieval and ARF processes.

2. Shiptrack Extraction Algorithm, Modifications and Data Filters

Figure 7 illustrates a typical extraction of a shiptrack from the satellite data. Brown (1995) provides the best explanation of the extraction process and algorithm particulars.

The extraction is a multi-step process to create a file that contains the radiative signature of the shiptrack and the surrounding ambient cloud. The shiptrack is first mapped by defining latitude/longitude points along its length. The algorithm linearizes the shiptrack then creates a 61 km swath about the track and assigns the centerline to the brightest pixels along the entire length. The algorithm then looks laterally out from the centerline to find the steepest reflectance gradient, which represents the edge of the track. At one kilometer beyond this gradient on both sides of the centerline, the next five pixels' reflectance values are averaged to produce the ambient cloud brightness for a 1 km length of track. This process is continued for each 1 km segment over the length of the track.

There are many measured and derived output parameters available from the algorithm. Some of these are: channel 1-5 values (eg., low 1, low 2, etc.) for both the shiptrack and the ambient cloud; various comparisons of inter-channel values 5, channel and shiptrack verses ambient values (eg., delta 3, DPC 3); width of the shiptrack; and total track length. The key parameters used here are: low 1, low 3, DPC 1 and DPC 3, shiptrack width, and length.

Modifications to the Nielsen and Durkee (1992) algorithm were needed to better study shiptracks as Gaussian dispersion plumes. A filtered width parameter (widthf) was added. It is the result of a 10 km running mean (the filter) applied to raw width values (i.e., distance between the dark pixels in Figure 7b) at every kilometer of the extracted track. Figure 11 illustrates the effectiveness of this parameter to filter out the small scale noise. The spikiness near the head of the track is due to the interaction with another shiptrack. The rapid increases near the end of the shiptrack are due to changes in the ambient stratus and age effects (i.e., dispersion causing a reduction of ship-produced aerosol concentration).

Another addition was the use of Channel 4 temperatures as an indicator of broken clouds. Unbroken stratus has very low variations in channel 4 temperatures. A broken stratus deck (standard deviation greater than 0.5 C) allows the temperature signal of the ocean surface to contribute and contaminate measured radiance. Therefore, pixel radiance values were set to null value when the standard deviation of ch4 was greater than 0.5 C. The final addition to the algorithm was code to calculate the horizontal plume dispersion parameter (σ_yOF). The letters following σ_y stand for the Opacity method which is used to calculate it, and the application of a Filter (same as the one used on width).

Some additional filtering and normalizing techniques were applied to the data to increase the effectiveness of the composite approach. A normalized down-track distance (Xnorm) was used to minimize variations in shiptrack radiative parameters caused by true wind (Ut) and relative wind (Ur) differences that exist between shiptracks. Ut is assumed
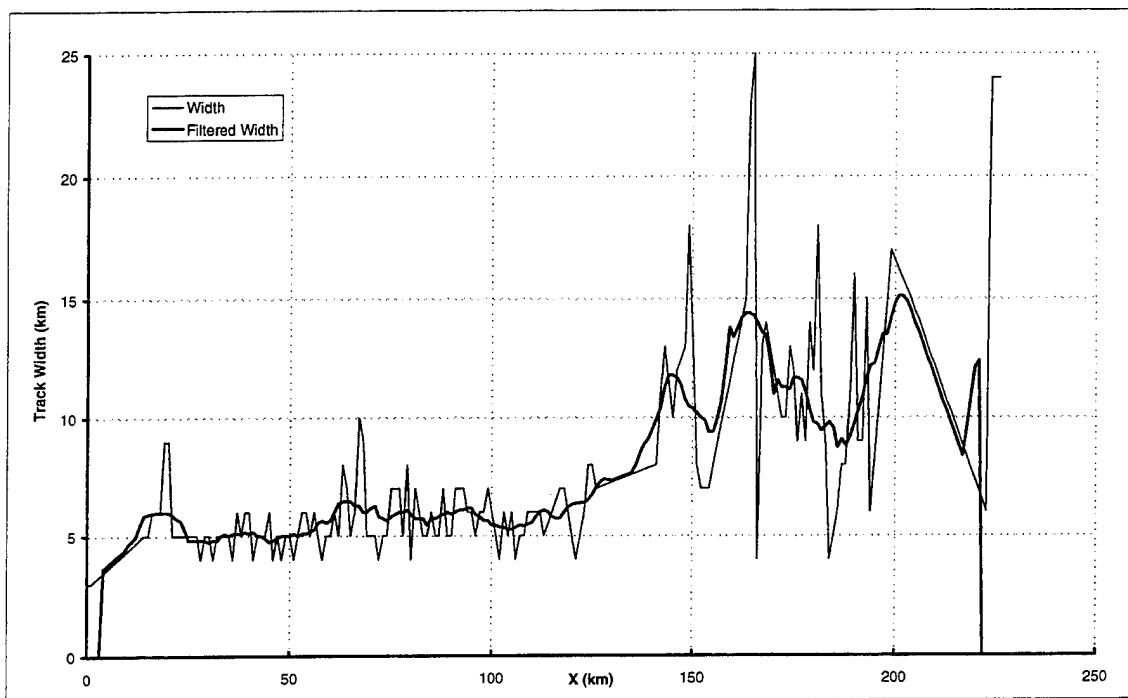
Figure 11. Example of how small scale noise in width measurements were filtered by using a 10 km running mean.

to drive turbulent dispersion, while Ur is assumed to incorporate the ships motion effects on shiptrack appearance. Again, the intent is to allow the side by side comparison of many different shiptracks.

Mathematically,

$$X_{norm} = \frac{U_t}{U_r} X$$

where X is the down-track distance calculated by the extraction algorithm. Ut accounts for the variations in turbulence that determine dispersive widening of the plume. We expect turbulence increases as the true wind increases. Ur removes the ship motion effects such that X/Ur gives the age of the track at distance X. This quantity is called time since emission (TSE).

3. Ship Characteristics

The vessel specific data listed in Appendix C was derived from four primary sources:

1. Lloyd's Register of Shipping 1992-1993.

2. The USCG's Marine Safety Information System (MSIS).

3. The Office of Naval Intelligence Merchant Ship Characteristics (MSC) publication.

4. The USCG's JSS.

The sources that provided the most data are listed first. MSIS and JSS data is available by on line computer queries. The other two sources are in hard copy form. No one source contained all the information. However, Lloyd's Register was by far the most complete.

4. Partitioning the Data

a. Shiptrack Dependencies and Assumptions

Basically shiptrack formation is a function of the ships' characteristics and environmental parameters. Each of these are composed of many more variables, some independent and others highly dependent upon one another. A partial listing of some ship variables includes: size, propulsion type, fuel type, power rating, and ship speed (Us). Propulsion type, power rating, speed, and Us are thought to be the most influential to shiptrack characteristics, and therefore were analyzed.

Some of the environmental variables include: diurnal effects, stratus cloud uniformity (brokenness), cloud microphysics [liquid water content (LWC), droplet concentration (N_d), droplet size (e.g., effective radius (r_{eff})), aerosol concentration and type], BLD, boundary layer stability, and Ut.

Some assumptions about the environmental parameters were necessary. We assumed constant LWC between the shiptrack and the ambient cloud. We assumed that cloud microphysical parameters (specifically r_{eff} and N_d) can be inferred from reflectance parameters. All shiptrack conducive MABLs were assumed to be well mixed with near-neutral stability and an overturning time on the order of one half hour.

b. Data Subsets

The data set was broken up into subsets to better isolate, understand and quantify the importance of the many variables that contribute to a shiptrack's radiative signature. Furthermore, subsetting enabled control of one (or more) variables at a time. This allowed the data to be grouped by propulsion type (steam turbine or diesel engine) and by power rating divisions (e.g., High ($\geq$ 23,500 kW), Middle (> 13,000 and < 23,500 kW), and Low ($\leq$ 13,000 kW)) The data subsets have titles of the form: Composite (number of shiptracks in the composite) - date range - time range - amplifying information. For example, the composite of all 131 shiptracks for the whole month of June 1995 has the title "Composite (131) - JUN94".

26

5. Prediction of Ship Characteristics

One of the motivations for this thesis was to determine if ship characteristics (namely propulsion type, and power rating) can be ascertained from shiptrack radiative properties. To that end a simple model was developed based on the far-field Gaussian dispersion equation. The model assumes power rating is proportional to source strength (Q). For larger power ratings the expected cloud response is an increase in droplet number and decrease in droplet size that should result in an increase in DPC 3. Therefore DPC 3 will decrease with increasing volume caused by increasing width and increasing relative wind:

$$DPC\ 3 \propto Q / (\sigma_y OF * U_r)$$

or

$$DPC\ 3 \propto Power\ rating / (\sigma_y OF * U_r)$$

Since DPC 3 is an observed quantity, power rating may be predicted through:

$$Power\ rating \propto \sigma_y OF * Ur * DPC\ 3$$

IV. RESULTS

After a brief description of the statistical parameters the results for the composite shiptrack are discussed. The outline of the discussion is: 1) shiptrack characteristics (signal) [broken down into three sections: environmental, radiative and physical] 2) sources and amount of variability (noise) and 3) summary and implications.

A. STATISTICS

From the data subsets listed above, composite plots of radiance parameters were created, and various statistical calculations were performed. The statistics included the use of regressions, correlations, analysis of variance (ANOVA), means, standard deviations and analysis of two samples of unequal size and variances (t-test). The trendline and equation in the plots are third order polynomial fits to the data. The coefficient of determination (R^2) value listed on many of the plots represents how well the trendline fits the data. In general the statistics helped to quantify the plotted results. Values that precede parentheses are composite means, i.e., averages of all the data for all shiptracks that are in that particular subset. The value in the parenthesis is the standard deviation for the preceding value. Appendix D provides a complete listing of the statistical results for each data subset.

B. COMPOSITE PLOTS AND DATA SUBSET ANALYSIS

1. Composite (131) - JUN94

Figure 12 presents composite plots of all 131 shiptracks (~30,144 data points) from 52 different ships. Collectively they represent nominal shiptrack characteristics from MAST. They also clearly define an envelope of variability for the plotted parameter. In other words, the trendline and subset statistics for a composite plot identifies the signal from the large variability (noise) inherent in the data. The reflectance parameters: low 1 (panel a), low 3 (panel b), DPC 1 (panel c), DPC 3 (panel d), and the physical parameters: widthf (panel e) and σyOF (panel f), are plotted verses normalized distance.

29
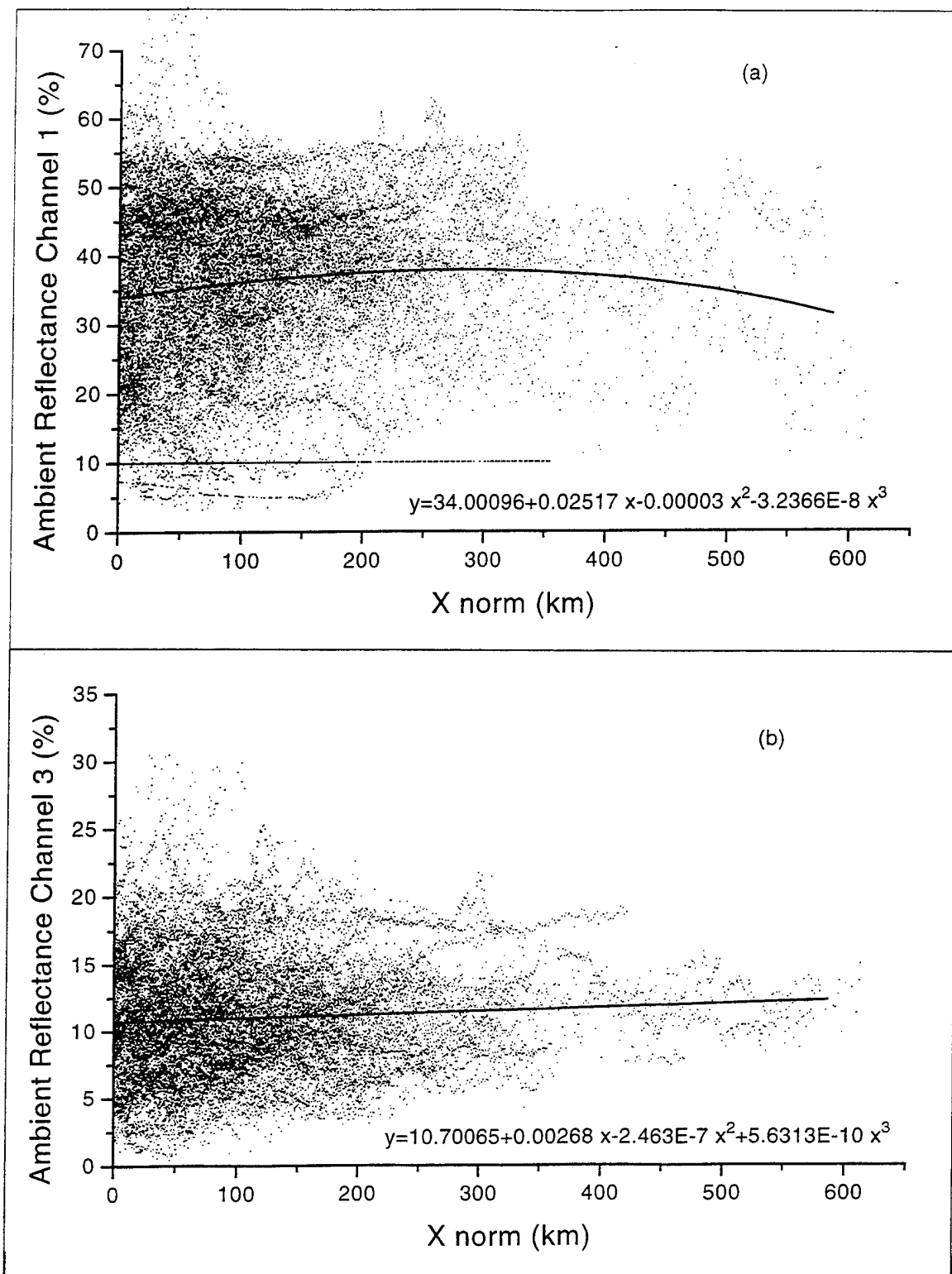
Figure 12. Composite plots of Ambient Reflectance (a) Channel 1 and (b) Channel 3 verses Xnorm for all 131 correlated shiptracks (52 ships, ~30,144 data points). The equation for the dark solid line (trendline) is included.

30
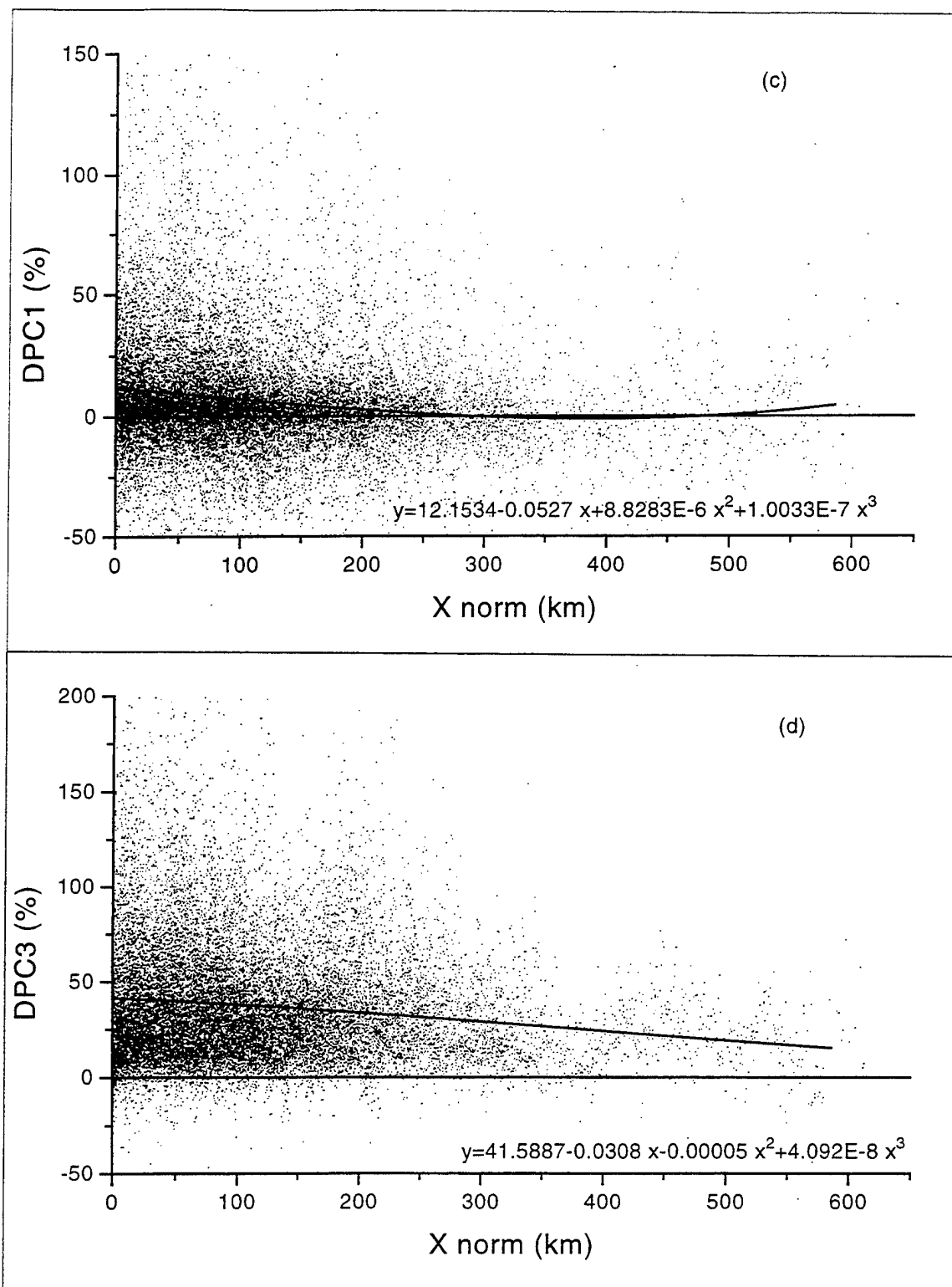
Figure 12. Composite plots of (**c**) DPC 1 and (**d**) DPC 3 verses Xnorm for all 131 correlated shiptracks (52 ships, ~30,144 data points). The equation for the dark solid line (trendline) is included.

31
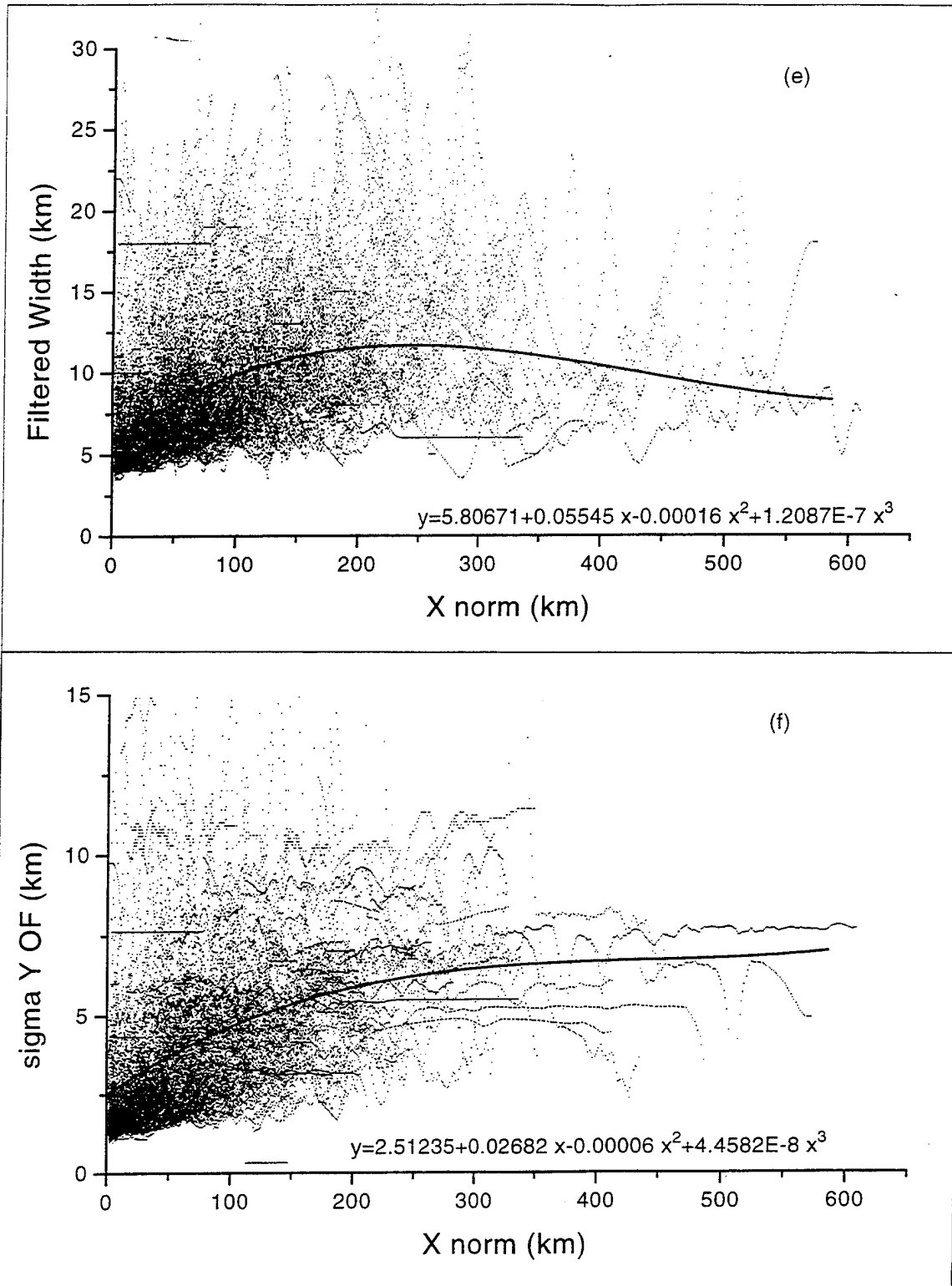
Figure 12. Composite plots of (e) Filtered Width and (f) σ_yOF verses Xnorm for all 131 correlated shiptracks (52 ships, ~30,144 data points). The equation for the dark solid line (trendline) is included.

The Y-axis values were picked to preserve the trendline information concurrent with showing the scatter in the data. All subsequent plots for a particular parameter were made with the same Y-axis values, whenever possible.

a. Environmental Signal

The trendlines in ambient channel 1 and 3 reflectance shown in Figure 12a and 12b have little to no slope along the shiptracks length. This result is expected because the background environment is not dependent upon down-track distance. The composite mean (standard deviation) values for ambient low 1, and low 3 are 36(12)% and 11(4)% respectively. Of note is the very large variability in low 1 for any given value of Xnorm. The large spread in the data (< 10% to > 55%) is strictly due to environmental factors. A shiptracks' radiative signature is superimposed on this background noise. Ideally the difference between the ambient and shiptrack values yields the contribution of the shiptrack. Practically however, the radiative signal to noise ratio is very small; the signal is best "seen" with DPC values vice difference values.

b. The Radiative Signal

The trendline for DPC in channel 1 in Figure 12c has a Y-intercept of 12.15%. This means that the near-head region of shiptracks are ~12% more reflective of solar radiation than the ambient cloud in which it formed. Increased reflectance decreases solar heating in the MABL which results in lower temperatures. Furthermore this brightening of shiptrack over the ambient extends to about 200 km down track. Thus the composite shiptrack on average creates a more reflective scene of ~1800 km^2 (using the average shiptrack width of ~9km). Upwards of 100 shiptracks have been observed in the stratus off the west coast on a shiptrack conducive day. Thus the area of increased reflectivity may exceed 180,000 km^2 which is about the size of the state of Florida. This is a significant finding, and has direct implications to the effects of aerosol pollution on radiation budgets, and the climate response.

The strong signal for DPC 3 seen in Figure 12d confirms that it is a better indicator of ship-induced effects on cloud microphysics than DPC 1. The trendline steadily decreases from a y-intercept of 41.6% to 25.5%. On average the radiation in the near-infrared is being reflected 1.37 times more than the ambient cloud.

c. The Physical Signal

The average track length is 296(232) km, which equates to an age of 7 hours 15 minutes (using the mean Ur of 22(8)kts). The average track width is 9(5) km. Figure 12e shows that shiptrack width increases with Xnorm to 250 km where it reaches a maximum of 11.7 km. It then decreases to about 8 km. The shape of the widthf trendline suggests that shiptracks have a dispersive nature similar to continuous point sources reported by Gifford (1985), and seen by Porch, et. al., (1990). The negative slope of the DPC 3 trendline also suggests that dispersion/diffusion processes dominate down track (temporal) characteristics. The filtering process removes the first 4 km of widthf data. It also effects the first few values of σ_yOF since it is dependent on width. This is being corrected to alleviate the problem in future work.

Figure 12f shows the horizontal dispersion parameter derived with the Opacity method and subsequently filtered (σ_yOF) as a function of normalized down-track distance from the source (long range) for a well mixed near-neutral boundary layer over water. The general shape of the trendline is similar to those reported in other dispersion studies over water (Skupniewicz and Schacher, 1986). However Skupniewicz and Schacher's curves stop at 12 km (they were not intended for long-range dispersion) and when extrapolated the curve values underestimate the values reported here by four to five times. Figure 13 shows σ_yOF data plotted on a Log Log plot verses time. Time is calculated from the head point of shiptracks ie., it does not include separation time (ST) that could add an average of 25 minutes to the age of each shiptrack. The dashed line is the Heffter (1965) equation ($d\sigma_y/dt = 1853$) which is predominantly used in long-range pollutant travel and dispersion predictions. The data exhibits the same slope as Heffter's equation. The close fit of measured data to Heffter line shows that the application of the Opacity method to shiptrack analysis is very successful.

34
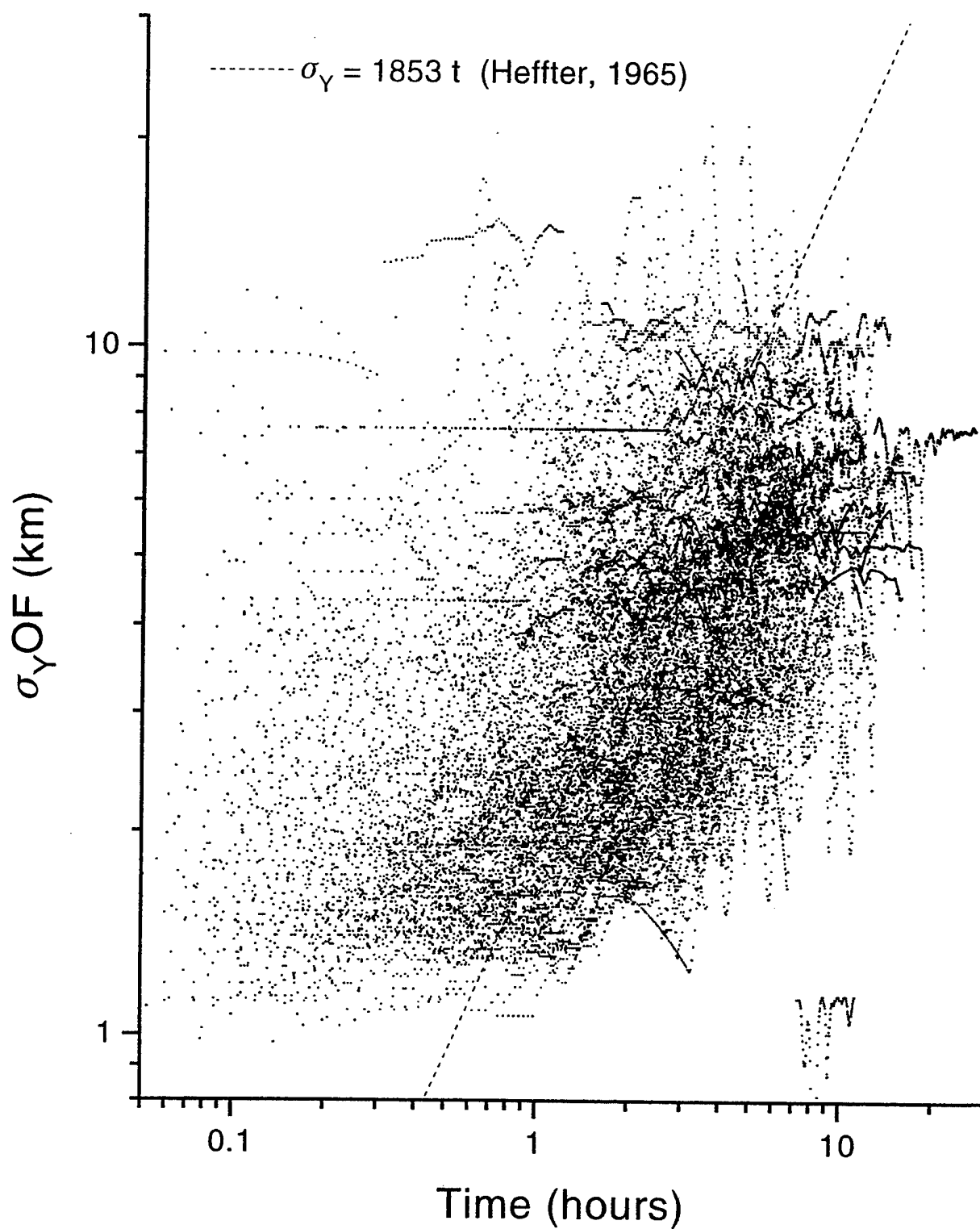
Figure 13. Composite Log Log plot of σ_yOF verses time. The dashed line is the Heffter (1965) equation often used in long-range dispersion predictions.

35

In fact the findings reported here represent a data rich (30,000+ data points), statistically significant characterization of long-range, over water diffusion from a continuous point source and should be utilized to improve pollution transport and dispersion models.

The variability seen in Figures 12 and 13 is quite large and could be due to: temporal effects from compositing a month of data; large scale spatial variations in the stratus deck (i.e., BLD differences between coastal and open ocean stratus); variations in the propensity of the 52 different ships to produce a shiptrack; or most likely a combination of all three. The composites that follow attempt to determine the source(s) of variability by reducing the number of independent variables.

2. Composite (5) - 29JUN94 - 1608UTC

If the variability is due to temporal effects alone, then limiting the data to one day (29JUN94) and one time (1608UTC) and a few shiptracks (one from each of the following ships: Hanjin Barcelona, Global Highway, Century Leader No 1, NYK Sunrise, and Star Livorno) should reduce the noise significantly. It did not. The standard deviations are only slightly lower, the means and plots (not shown) are reasonably close to those for the Composite (131) - JUN94 case. For example, DPC 1 and DPC 3 standard deviation values for this composite are: 21.36% and 26.22% as compared to 26.25% and 33.98% for Composite (131) - JUN94. Thus, most of the variability must be due to the variations in the ship characteristics and/or variations in the stratus deck that is occurring on a scale smaller than the distance between the ships in this composite.

3. Composite (5) - 29-30JUN94 - 14 h - Hanjin Barcelona

Shiptracks for one ship were composited to determine the contribution of ship characteristics to variability. If ship to ship differences are causing the variability, then holding these characteristics nearly constant will greatly reduce the variability in the data. Figure 14 shows the composite plots for the Hanjin Barcelona. The five shiptracks in this composite span 14 hours during the 29-30 of June. The shape and general characteristics of these plots agree quite well with those previously presented. The standard deviations for this single ship composite are about the same or more than those of the previous two

36
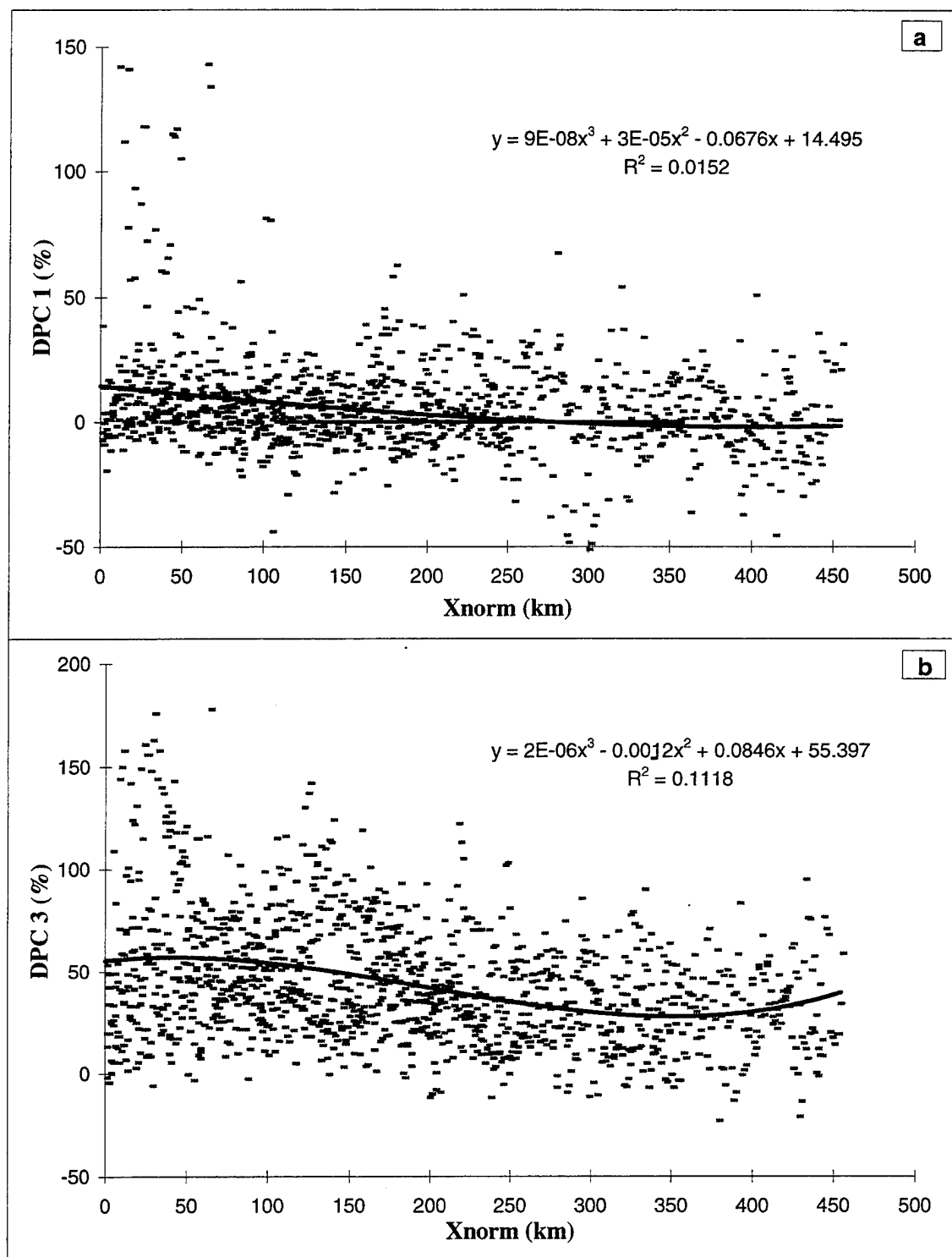
Figure 14. Composite plots of (**a**) DPC 1 and (**b**) DPC 3 verses normalized distance for shiptracks correlated with the Hanjin Barcelona over 14 hours on 29-30JUN94. The equation for the dark solid line (trendline) and its R squared value is included.

37
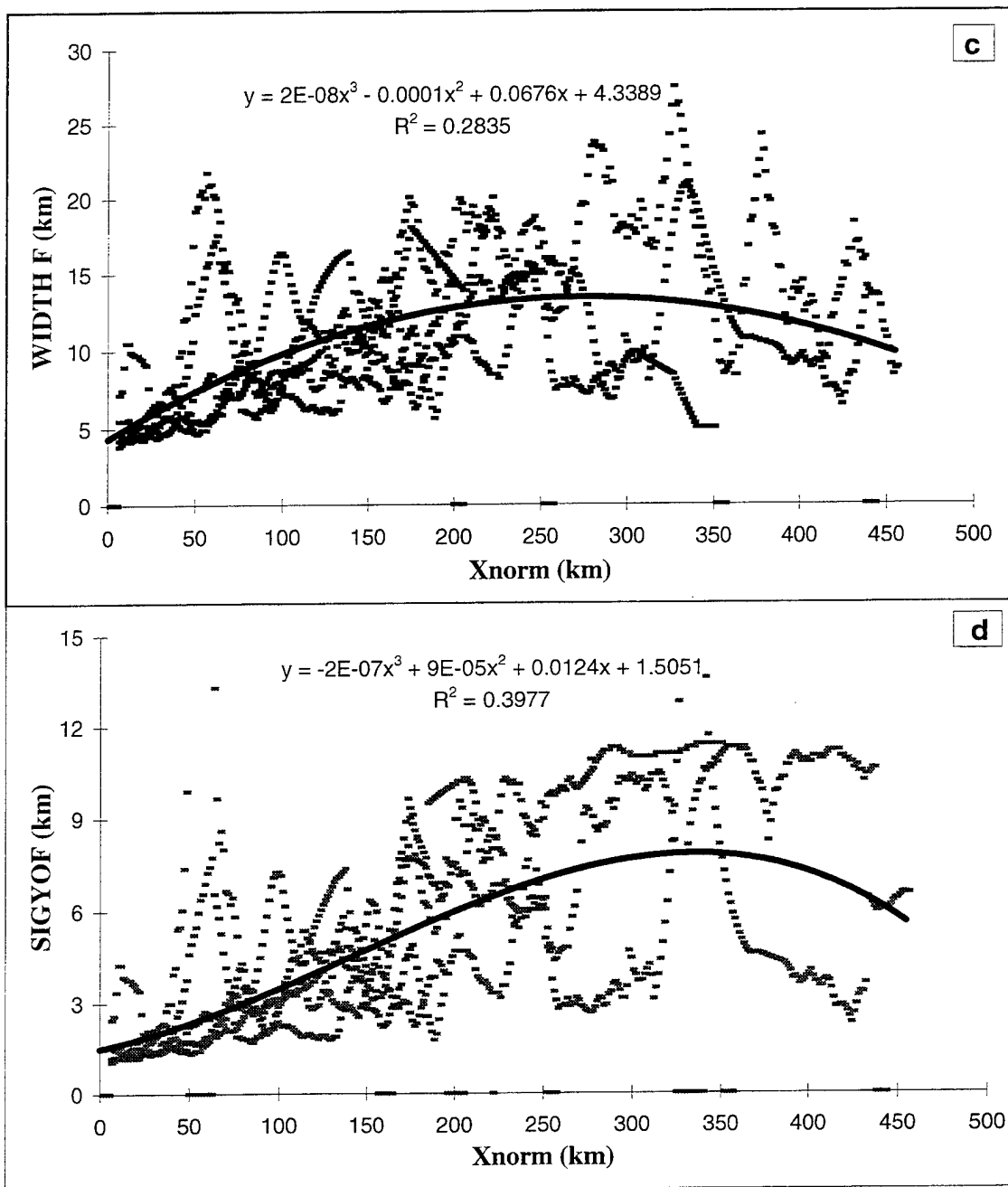
Figure 14. Composite plots of (c) Widthf and (d) SigmaYOF verses normalized distance for five shiptracks correlated with the Hanjin Barcelona over 14 hours on 29 30JUN94. The equation for the dark solid line (trendline) and its R squared value is included.

38

composites. See Appendix D for specific values. The sinusoidal variations seen in Figure 14c, d indicate that the variability could be due to the cloud structure and/or plume meanders and that they occur on a spacial scale of about 10 to 25 km. Thus two conclusions can be drawn. Ship effects are of some importance in determining radiative characteristics and variability, (that is, the signal remained and the noise was only slightly reduced or not reduced at all) and variability is forced predominantly by environmental factors. Careful analysis of other single ship composites gave the same result. Quantifying this effect is the goal of the next data subset.

4. Composite (2) - WCHF, KNIJ - 12JUN94 - 1535UTC - Identical Ships

This subset controlled nearly all of the ship and environmental variables. It is composed of two shiptracks from two ships which have identical characteristics, at the same image time, in nearly the same location (only 138 km apart). Figure 7a shows the shiptracks correlated to the Manulani (KNIJ) and Sea-Land Consumer (WCHF). See Appendix C for their ship characteristics. They were both on the same course (256 degrees) doing the same speed (22 kts) and therefore produced the same Ur (26.9 kts).

Figure 15 shows the variability in the DPC 3 values for each ship individually plotted verses X. (X is used vice Xnorm because Ut and Ur are assumed to the same since both ships are in close proximity and have the same course and speed.) Note the difference in the shape of the trendlines and the variability about them. Figure 16 shows the line plot of DPC 3 verses X for these two shiptracks. The spikes and general patterns are qualitatively quite similar. An analysis of variance test showed that quantitatively they are not. The larger peaks (KNIJ 0-25 km, and 100-140 km, WCHF 80-120km) are due to the shiptrack crossing with other shiptracks in the area. The large dip in KNIJ's value at about 90 km is due to cirrus contamination. Regression analysis of the data gave a correlation coefficient (R) of 0.392 and a R^2 value of 0.1537. In other words about 15% of the variability in one shiptrack can be accounted for or explained by common influences on both shiptracks. This value is much lower than expected based on the assumption that most environmental conditions were equal and the ships nearly identical.
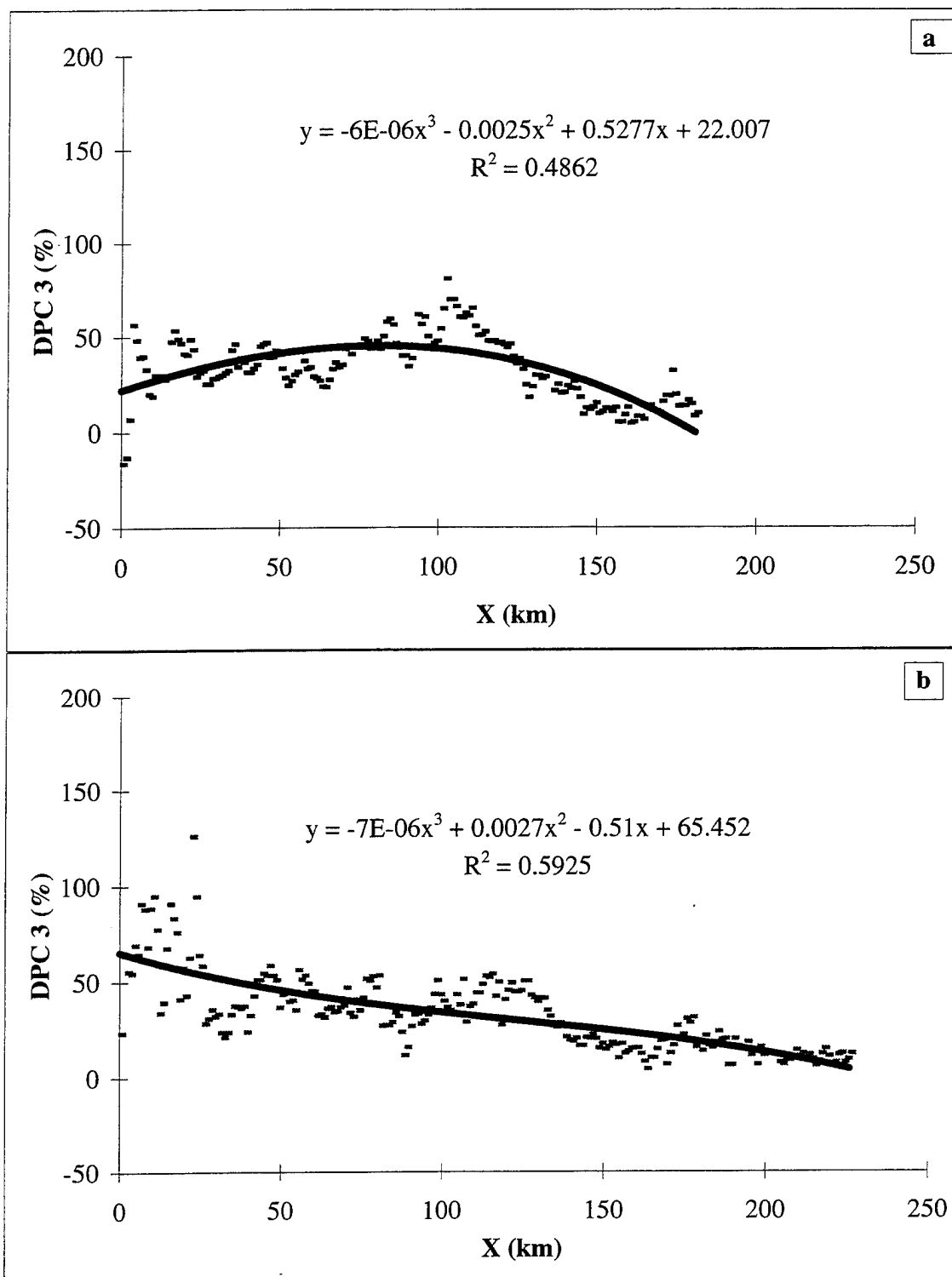
Figure 15. Variability and trends in DPC 3 verses X for (**a**) Sea-Land Consumer (WCHF) and (**b**) Manulani (KNIJ) on 12JUN94 at 1535 UTC.

40
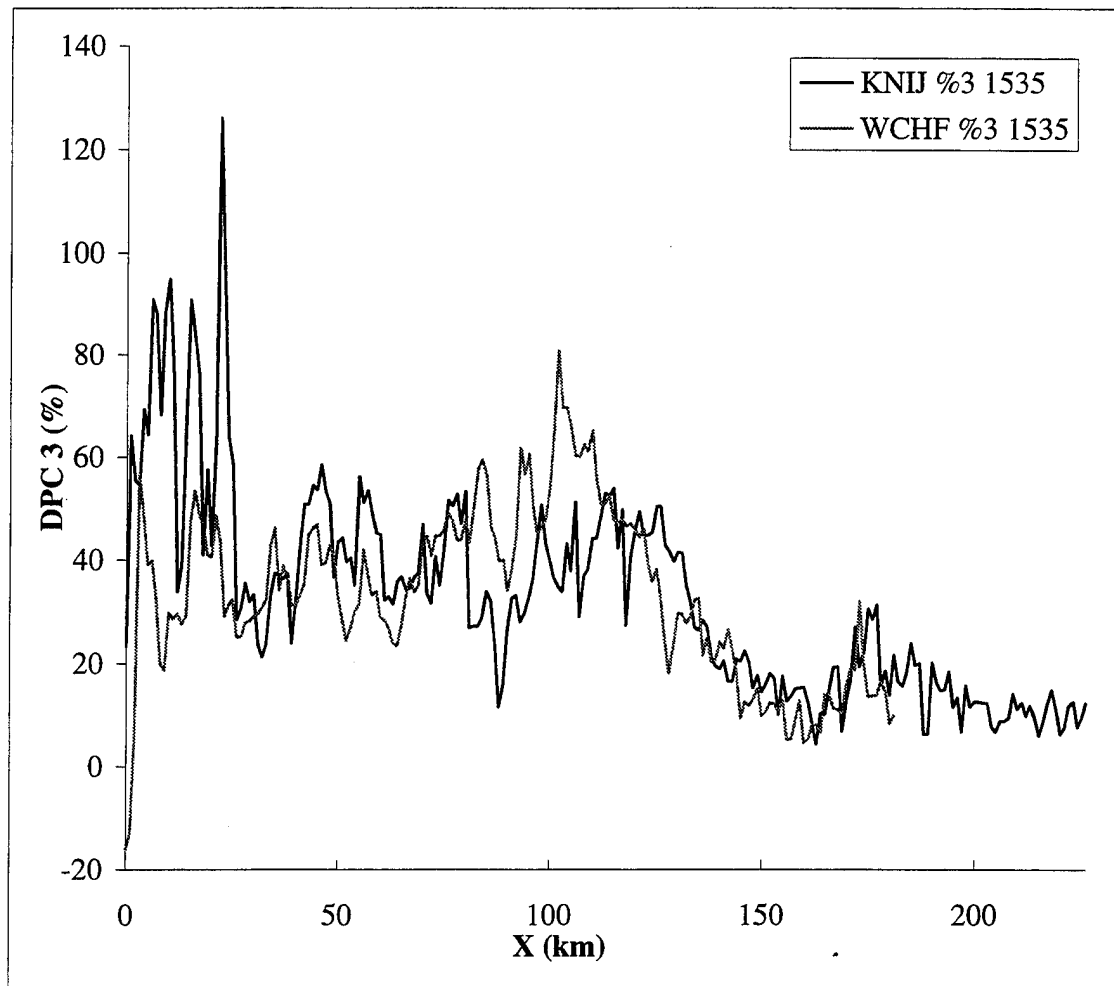
Figure 16. Line plot of DPC 3 verses X for Sea-Land Consumer (WCHF) and Manulani (KNIJ) shiptracks on 12JUN94 at 1535 UTC.

Apparently, the other 85% of the variability is due to unmeasured environment and ship characteristics. Most likely the variability is due to irregularities in the stratus on a scale smaller than the distance between the two ships e.g., large eddy scale variations.

Figure 17 shows the composite plots for these two shiptracks. The trendlines have the same shape as those previously presented and the means are not significantly different. The standard deviations on the other hand are about half as large. This indicates that the environment variables are the primary driver of variability in shiptracks radiative signature. The next question to investigate is whether differences in ship characteristics produce enough of a signal to be determined radiatively.

5. Ship Characteristics (Steam vs Diesel & Power Rating)

Shiptracks correlated to steam turbine ships were separated out from those produced by diesel engines. Composite plots (not presented; they have the same general trends as above) and composite statistics were generated. Table 2 shows the important statistical results. Appendix D contains a complete listing of the composite statistics.

		PROPULSION TYPE			
	Variable	Diesel	Steam	Difference	Ratio
ENVIRONMENT	$low1_{amb}(\%)$	36.35	32.90	3.45	1.10
	$low\ 3_{amb}(\%)$	11.07	10.45	0.62	1.06
PHYSICAL	Length(km)	301.6	254.6	47.0	1.18
	Age (hr)	7.5	5.7	1.78	1.18
	Width (km)	9.32	8.00	1.32	1.16
	$\sigma_y OF$ (km)	4.51	3.91	0.60	1.15
RADIATIVE	DPC 1 (%)	6.23	11.25	-5.02	0.55
	DPC 3 (%)	36.33	40.42	-4.10	0.90

Table 2. Statistical Comparison of Propulsion Type Effect on Shiptracks.

The values in Table 2, 3 and 4 were statistically analyzed for two samples of unequal size and variance (t-test) test and were found to be statistically significant (> 99% confidence interval). [Note the values in parentheses that follow are no longer standard
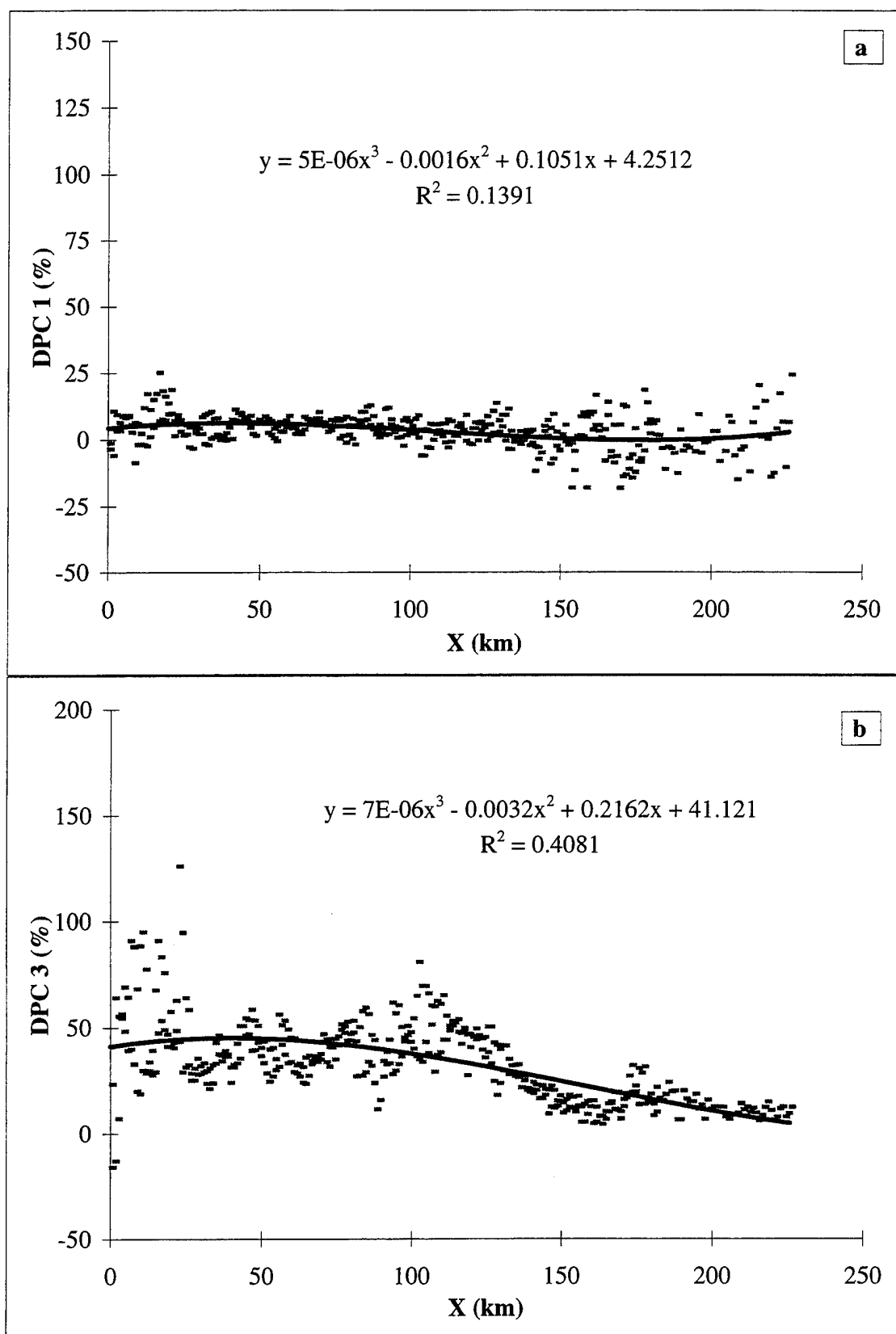
Figure 17. Composite plots of (**a**) DPC 1 and (**b**) DPC 3 verses X for Sea-Land Consumer (WCHF) and Manulani (KNIJ) on 12JUN94 at 1535 UTC.

Figure 17. Composite plots of (**c**) widthf and (**d**) sigma YOF verses X for Sea-Land Consumer (WCHF) and Manulani (KNIJ) on 12JUN94 at 1535 UTC.

44
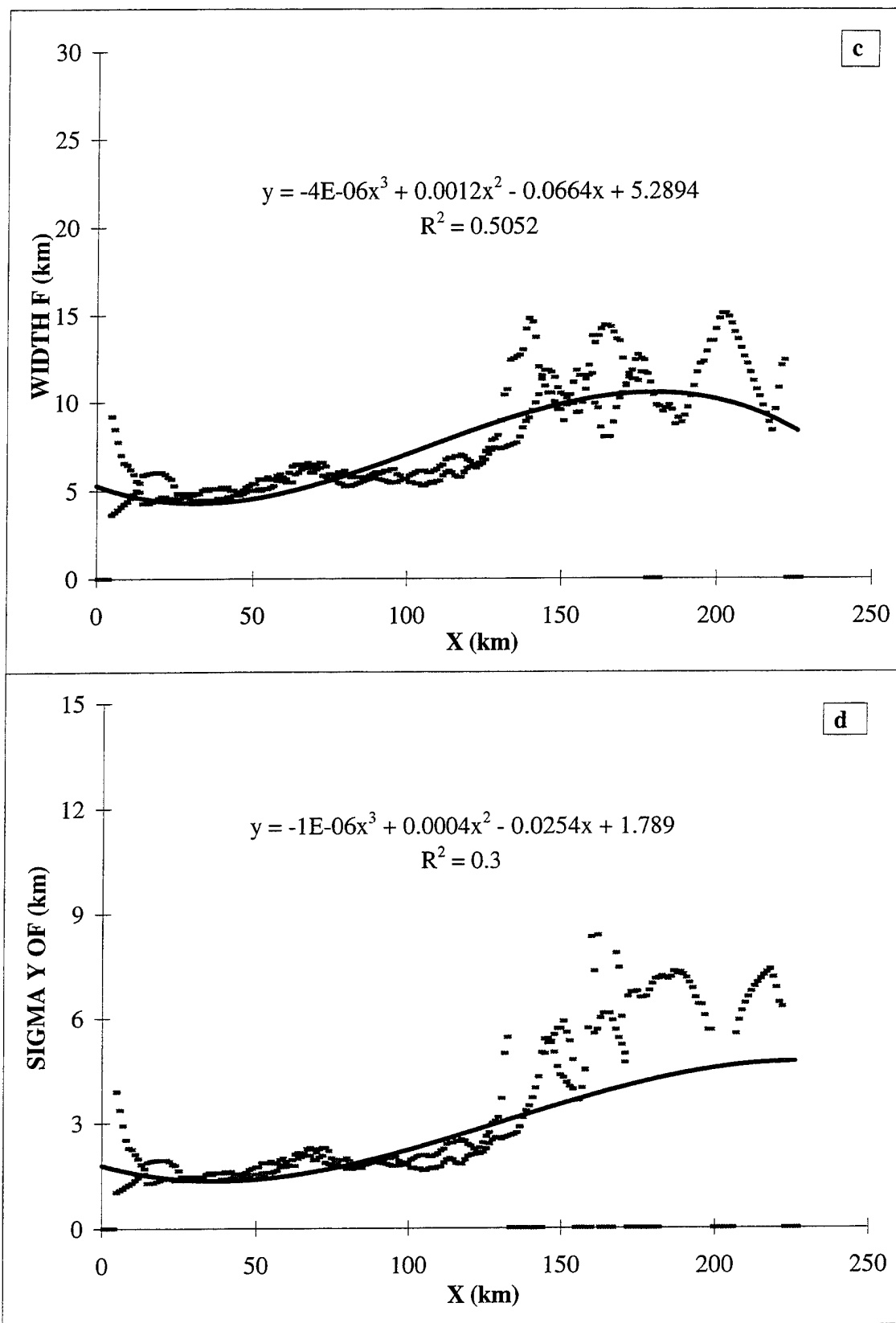
deviations but rather the difference between the items compared.] In summary, steam turbine ships tend to produce shiptracks that are 1.78 h younger, 1.18 times shorter (47 km), 1.16 times narrower (1.3 km), 1.81 times (5.02%) more reflective for DPC 1, and 1.11 times (4.10%) more reflective for DPC 3 than shiptracks correlated with diesel engine propulsion systems. The maximum width for the composite steam shiptrack is 1 km narrower than diesels and occurs about 100 km closer to the head. These results imply that the aerosols produced by steam turbine ships are different than those from the diesel ships, and resulted in the differences in the shiptrack's radiative and physical features. In-situ measurements from the instrumented aircraft will be able to confirm this.

A ships power rating has a measurable impact on the radiative and physical characteristics of the shiptrack it produces. The data was broken up into three power rating subsets e.g., High (≥ 23,500 kW), Middle (> 13,000 and < 23,500 kW), and Low (≤ 13,000 kW). Appendix D lists the complete results of the composite statistics. Table 3 summarizes the key results.

		POWER RATING			
	Variable	High kW	Low kW	Difference	Ratio
ENVIRONMENT	$low1_{amb}(\%)$	38.92	33.15	5.77	1.17
	$low\ 3_{amb}(\%)$	10.88	10.87	0.01	1.00
PHYSICAL	Length(km)	314.5	262.7	51.8	1.20
	Age (hr)	7.25	6.61	0.63	1.10
	Width (km)	9.77	9.02	0.75	1.08
	$\sigma_y OF$ (km)	4.80	4.56	0.24	1.05
RADIATIVE	DPC 1 (%)	4.76	7.61	-2.85	0.63
	DPC 3 (%)	38.06	34.69	3.37	1.09

Table 3. Statistical Comparison of Power Rating on Shiptracks.

In summary, ships with High total designed shaft power ratings produce shiptracks that are 1.1 times (.63 hrs) more persistent, 1.2 times (52 km) longer, 1.08 times (.75 km) wider, 1.61 times (-2.86%) less reflective in DPC 1, and 1.09 (3.37%) more reflective in DPC 3 than Low power rating ships. These results suggest that larger kW ships produce more aerosols. The aerosol and CCN concentration is therefore higher in the cloud which results in reduced droplet size and elevated brightness.

The power rating difference between the steam turbine ships is small. The range in diesel ships is large. The Middle power rating subsets for each propulsion type were statistically compared and listed in Table 4. This tested if power rating differences alone caused Table 2 results.

	MIDDLE POWER RATING (>13,000, <23,500 kW)			
	Variable	Diesel	Steam	Difference	Ratio
ENVIRONMENT	$low1_{amb}$(%)	35.5	18.42	17.09	1.93
	low 3_{amb}(%)	11.3	6.64	4.66	1.70
PHYSICAL	Length(km)	313.9	187.1	126.8	1.68
	Age (hr)	11.09	2.99	8.1	3.71
	Width (km)	8.81	6.63	2.18	1.32
	$\sigma_y OF$ (km)	3.98	3.75	0.23	1.06
RADIATIVE	DPC 1 (%)	8.42	55.38	-46.96	0.15
	DPC 3 (%)	38.30	97.95	-59.65	0.39

Table 4. Statistical Comparison of Steam verses Diesel Shiptracks: Middle Power Rating.

Table 4 results confirm that ships powered by steam turbines produce shiptracks that are significantly different (radiatively and physically) than shiptracks produced by diesel propulsion ships.

C.   MODEL

A model (described in chapter III) was developed to determine a ships power rating from its shiptrack characteristics. Once again, the model has the form:

$$Power\ rating \propto Ur * \sigma_y OF * DPC\ 3$$

Figure 18 is a three dimensional depiction of the model results. The vertical axis is the predictand (kW). The horizontal axis show three range bins. Ambient low 3 reflectivity is used to classify environmental conditions. Power rating is the other horizontal axis it is used to check model results. The strongest result is seen in the clean environment (low 3 ambient <8%), where model values increase in accordance with actual increase in kW. However, in the moderately clean (8-12%) and dirty (>12%) ambient environments the model is inconclusive. Furthermore, for a specified kW bin the model should predict the same value regardless of ambient reflectance. It does not. The model output is dominated by the DPC 3 variable which is highly dependent upon the background environment.
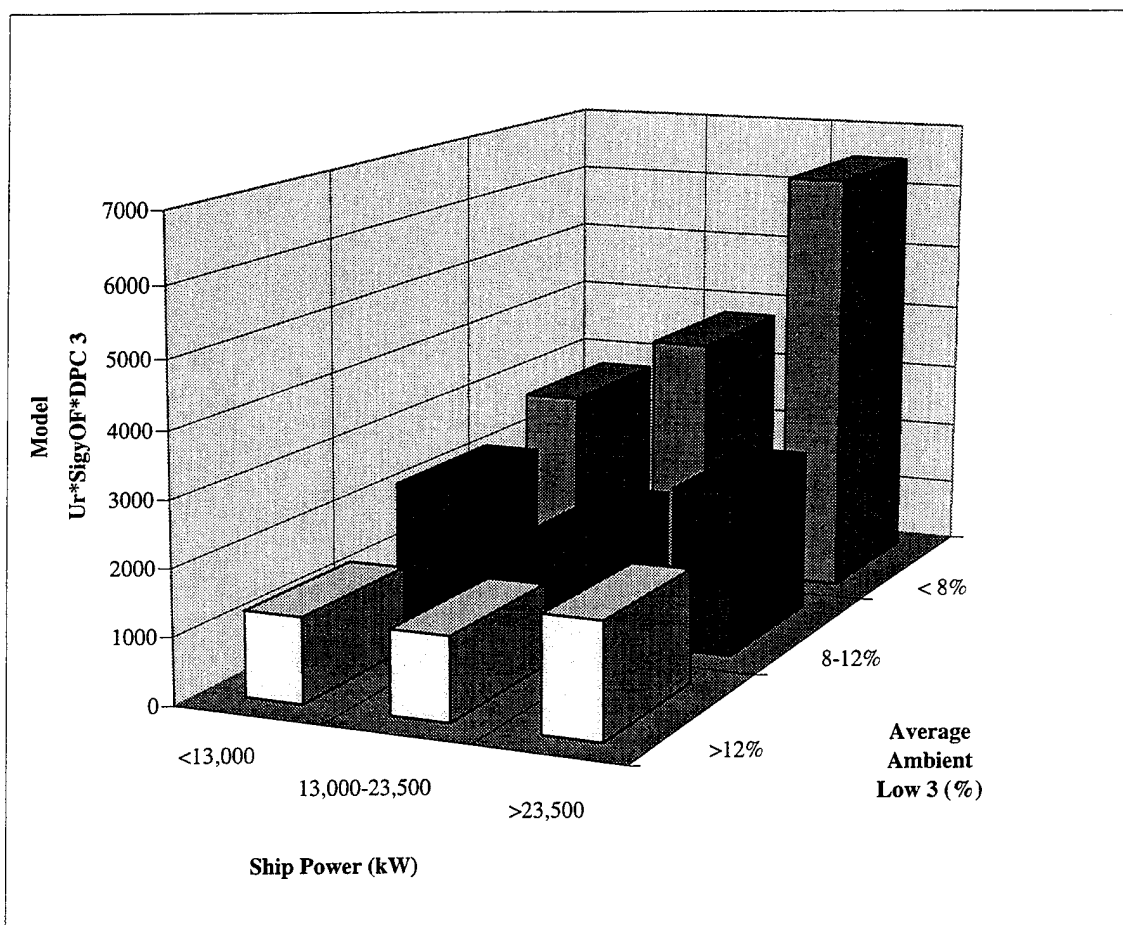
Figure 18. Results of the modified Gaussian dispersion model used to predict ship power rating. Results sorted by average ambient channel 3 reflectivety (low 3).

V. CONCLUSIONS AND RECOMMENDATIONS

A. CONCLUSIONS

This shiptrack study represents an ambitious attempt to describe and quantify shiptrack characteristics; and to predict some of the characteristics of the ships that cause them. It utilized a composite approach on a statistically significant set of 131 correlated shiptracks from the MAST experiment which was conducted off the California coast during the month of June 1994. The data set includes a wide range of ship and environmental variables which often combined to cause large variability or "noise" in the data. The composite technique successfully determined the ship-induced radiative signature or "signal" from the highly variable ambient noise.

Figure 19 illustrates **composite shiptrack characteristics** of important *environmental, radiative,* and *physical* parameters determined. Figure 19 also lists some important summary statistics; a more complete list is found in Appendix D. In summary, the composite shiptrack is 296 km long, about 7.3 hours old, averages 9 km wide, has a separation distance of 16 km, and a separation time(ST) of 25 minutes. It formes in a ambient environment with a Ut of 15 kts and a low 3 radiative signal of 11%. The radiative signal of the composite shiptrack is, low 3 reflectance equal to 14% with DPC 1 and DPC 3 values of 7% and 37% respectively.

The large data set was broken up into subsets to provide a means to isolate and quantify sources of variability in the radiative signal. Composite (2) - 12JUN94 - 1535UTC is the most controlled subset. It contained shiptracks from the same image from two identical ships who were only 138 km apart, on the same course, same speed, and under the same stratus. Correlation and regression statistics between the shiptracks from this subset showed that although the shiptracks trendlines looked very similar only 15.4% of the variability in one ships signature could be also seen in the others. That is to say, the remaining 84.6% of the variability is most likely due to environmental variability occurring on the large eddy scale. Thus ambient variability is greater than five times the ship-induced variability, at least for this case.
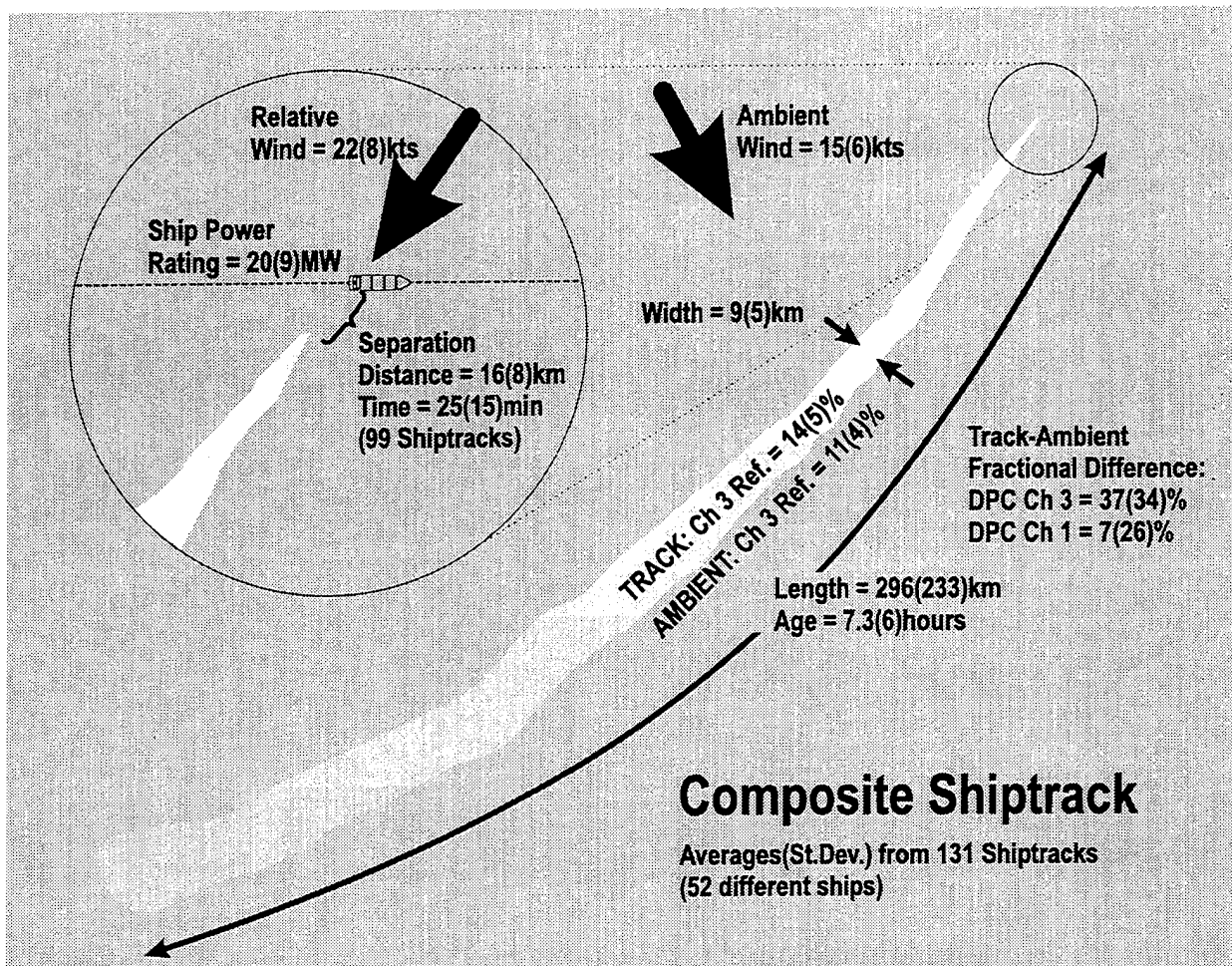
Figure 19. Composite Shiptrack Characteristics from 131 Correlated MAST Shiptracks.

Predictability of key ship characteristics (propulsion type, and power rating) from shiptrack radiative signature was investigated. The composite plots and statistics show strong qualitative and quantitative correlations between propulsion type and power ratings and the shiptrack physical and radiative parameters. In summary, steam turbine ships tend to produce shiptracks that are 1.78 h younger, 1.18 times shorter (47 km), 1.16 times narrower (1.3 km), 1.81 times (5.02%) more reflective for DPC 1, and 1.11 times (4.10%) more reflective for DPC 3 than shiptracks correlated with diesel engine propulsion systems.

Ships with High total designed shaft power ratings ($\geq$ 23,500 kW) produce shiptracks that are 1.1 times (.64 hrs) more persistent, 1.2 times (52 km) longer, 1.08 times (.75 km) wider, 1.61 times (-2.86%) less reflective in DPC 1, and 1.09 (3.37%) times more reflective in DPC 3 than Low power rating ($\leq$ 13,000 kW) ships. These results suggest that larger kW ships produce more aerosols. The aerosol and CCN concentration is therefore higher in the cloud which results in reduced droplet size and elevated brightness.

The modified Gaussian dispersion model provided reasonable prediction of ship power rating in a clean ambient environment. It was not a good predictor in dirtier backgrounds. The model is too dependent upon one variable (DPC 3) which in turn is highly dependent upon the cleanliness of the background environment. An ideal model should predict power rating regardless of ambient conditions. Nonetheless, the model does provide a foundation for future research.

The second goal of this thesis was to quantify the radiative effects of anthropogenic aerosols in marine stratus clouds. Mean DPC 1 values from Composite (131) - JUN94 show that on average shiptracks are about 7% more reflective in the solar wavelengths than the ambient cloud they formed in. Near the head of the track the mean DPC 1 values are about 12%. This increase is substantial over a limited area (~1800 km^2), but has global implications. Modelers of pollution and its effects can surely use this quantitative result to better understand the effect of anthropogenic aerosols on regional and global radiation budgets and climate response. The secondary effects of

shiptracks (persistence and indirect aerosol forcing on cloud formation and reflectivity) is likely to be present as well. According to Coakley et al. (1987) the effect of aerosols on the earth's radiation budget through their influence on clouds may be several times that of the direct interaction of the aerosol with solar radiation.

The application of the opacity method to shiptrack analysis was very successful. Figure 12f and Figure 13 represent a data rich (30,000[+] data points), statistically significant characterization of long-range, over water diffusion from a continuous point source. The curves were developed from measurements of aerosol diffusion in a near-neutral stability MABL which was capped by a subsidence inversion. They match closely with the analytical results presented by Heffter (1965) for long-range pollutant travel and dispersion. These curves will be refined and undoubtedly will be used in future pollution transport and diffusion models.

The third goal of this thesis was to test three MAST hypotheses. If submicron aerosol particles from ship stacks were not responsible for cloud droplet and radiative features of shiptracks then the statistically significant results that are reported would not have been possible. The shiptrack radiative signature is distinct and positively correlated to both propulsion type and power rating. Each of these ship characteristics apparently dictates, to a noticeable degree, the resultant shiptrack radiative signature. The only physical way that this could be uniformly true for all the environmental conditions during MAST is if the ships exhaust composition (e.g., aerosol size, concentration, and distribution) are different. The in-situ data from the MAST aircraft sensors should confirm this deduction.

Gas-to-particle conversion and particle accumulation may provide a source of CCN for cloud modification downtrack. DPC 1 trendlines asymptotically approaches zero. DPC 3 values generally have a negative slope also. The negative slopes suggest that CCN additions downtrack is not occurring. However some of the smaller composites showed a slight positive slope in the DPC 3 trendlines to about 50 km {~1.7 hours (ST=25 minutes plus 1.25 hours for the 50 km assuming average Ur=22kts)}. The slight

increase may be due to gas-to-particle processes but also may be due to normal diffusion processes and the time it takes for the cloud microphysical properties to respond to the injected aerosols.

Heat and moisture injection from the ship stack may enhance buoyancy and vertical motion affecting (a) cloud formation and (b) the delivery of aerosol to the cloud base. The average separation time of 25 minutes is consistent with natural boundary layer mixing processes. This does not imply that the ship effluent is mixed more rapidly due to heat and moisture effects on buoyancy.

B.   RECOMMENDATIONS

1. Data Collection/Correlation Process:

- Order JSS ship position data for a block of time (i.e., a whole month) rather than performing very time consuming queries (4-6 hours of work to get one day of position data).

- DR ships to the image times and overlay these positions on the appropriate image for final correlation based on orientation criteria.

- Obtain BLD for each correlation.

- Create a subset of shiptracks that are not contaminated by cirrus, cloud thinning, or shiptrack crossings. This would be the cleanest subset of shiptracks, from which the ideal composite shiptrack and its characteristics could be determined.

2. Algorithm Changes:

- Integrate the reflectance values across the shiptrack vice taking the brightest pixel and the one pixel on either side to define track centerline.

- Enlarge the ambient averaging scheme from six pixels (three km on either side of the shiptrack) to 20 km (ten pixels on both sides of the shiptrack). This would make the ambient sample size on both sides of the shiptrack at least as large as the average width of shiptracks.

- Apply more aggressive filters (25+ km running means vice the 10 km application used here).

53

3. Analysis:

- Compare the results found here with the in situ measurements obtained by MAST instrumented aircraft. This will help verify the conclusions that ships aerosols have a significant impact on cloud microphysical characteristics which can be clearly detected radiatively.

- Develop correlation coefficients which will link radiative parameters to the microphysical parameters.

- Perform a negative results test. That is, use uncorrelated ship position reports in a known shiptrack conducive environment to investigate why no shiptrack were formed by the ships. This may lead to the determination of the aerosol concentration threshold for shiptrack detection.

4. Model:

- Apply existing long range dispersion model parameters to improve the modified Gaussian dispersion model developed.

- Add independent variables (maximum width, downtrack distance to the maximum width, shiptrack length, BLD and different radiative parameters are a few that might show better results).

- Revisit the assumptions and substitutions made, establish some coefficients to convert the model output to actual kW values instead of a qualitative result.

5. Miscellaneous:

- Make shiptrack composites from the same ship covering hours, days, months, years to further quantify the environmental effects. Ships with multiple year shiptrack correlations are Keystone Canyon (KSFK), and NLVS from Pettigrew (1992), and WNRD, 4XGV, PGLA, WRYC, JKLS, and WRJP from Mays (1993).

APPENDIX A. OPACITY METHOD APPLIED TO SHIPTRACKS

Charles E. Skupniewicz

In the study of the shiptrack phenomenon, the remotely-sensed brightness and width of the track is partly controlled by dispersion of cloud condensation nuclei originating from the ship's stack, but also depends on the cloud microphysics, source composition and strength. One goal of shiptrack research is to estimate the dispersion of the track so that cloud microphysical changes and source characteristics can be better understood.

Many atmospheric dispersion models require an estimate of the dimensions of a plume or puff. These estimates are most reliable if based on experimental data collected under conditions and downwind ranges similar to those being modelled. Therefore, much research has been devoted to the measurement of dispersion patterns and parameterization of plume growth using tracer gases. Most of these experiments have been performed over land; very few over water, fewer yet at the downwind ranges where shiptracks appear. At these ranges, horizontal dispersion most important, but it is primarily controlled by mesoscale variability. Therefore, plume growth parameterizations derived from other experiments may not apply.

Based on these goals and limitations, it is desirable to develop a method for estimating horizontal plume parameters directly from the observed brightness patterns of the track which is independent of the source characteristics or cloud microphysics. A technique termed the "opacity method" introduced by Roberts (1923) and applied to dispersion studies by Gifford (1957,1980) possesses these qualities. The method was developed to estimate dispersion parameters from smoke plumes as tracers. While the ranges studies in these early experiments were vastly different than those where shiptracks occur, the fundamental assumption required is equally valid; i.e. the visible edge of the plume represents a constant threshold of particle density along the line of sight. Shiptracks are visible because the size of cloud droplets is smaller within the track than in the ambient. Making the assumption that liquid water content is constant in the shiptrack domain, a larger concentration of cloud droplets is expected in the track. It seems reasonable to assume that the shiptrack becomes visible at some threshold of droplet concentration. While the relationship between reflectivity and droplet concentration may vary significantly at other points in the shiptrack, it is only required that the detectable edge represents a fixed level of

concentration. This assumption is not strictly enforced when changes in the ambient cloud along the track are significant. We address problems introduced by this noise source later in this document.

Accepting the primary assumption, we derive the opacity equation for the shiptrack case. The "far field" form of the gaussian plume model for a fixed continuous source in a well-mixed boundary layer is

$$C(x,y) = \frac{Q}{\sqrt{2\pi}UH\sigma_y} e^{-\frac{y^2}{2\sigma_y^2}}$$

where C is concentration, in this case, cloud condensation nuclei, Q source strength, H mixed layer depth, σ_y is the horizontal plume dimension, and x,y is the down-track and cross-track coordinates. Shiptracks are advected with the relative wind, therefore, U is the mean relative wind speed.

Let y_e be the cross-track position where the track is first visible, or the edge. Let ρ be the maximum value of y_e. Then differentiating with x gives

$$\frac{d}{dx}C(y) = \frac{Q}{\sqrt{2\pi}UH\sigma_y} e^{-\frac{y^2}{2\sigma_y^2}} [-\frac{dy_e^2}{dx} + (\frac{y_e^2-\sigma_y^2}{2\sigma_y^2})\frac{d\sigma_y^2}{dx}]$$

so that at ρ, $dC/dx = dy_e/dx = 0$, and $y_e = \sigma_y$. Substitution into equation 1 gives

$$C(y) = \frac{Q}{\sqrt{2\pi e}UH\rho}$$

Anywhere along the plume, the following equation holds defining the horizontal plume parameter:

$$\sigma_y^2(x) = y_e^2 [\ln(e\rho^2) - \ln\sigma_y^2(x)]^{-1}$$

This equation states that σ_y is a function of the edge of the plume and the maximum width of the plume only, with no dependency on source strength, wind, or mixed layer depth, and no assumption about the along track variation of the plume parameter. Figure 5 illustrates a simplified view of the track. For $x < x(\rho)$, σ_y is less than y_e. For $x > x(\rho)$, σ_y is larger than y_e, and y_e quickly approaches 0.

We encountered three difficulties in implementing this scheme. First, the solution is iterative and 2 solutions exist for σ_y. This is easily solved by choosing an initial guess based on x; i.e. if $x < x(\rho)$ guess small and if $x > x(\rho)$, guess large.

The second problem was the choice of ρ. When using the simple maximum of all width values, the solution gives unreasonably small values for small x and very large values for $x > x(\rho)$. A large inflection occurs on either side of $x(\rho)$. This problem is primarily a result of inhomogeneities in the background stratus field, and was remedied as follows. Assume the track width "signal" responds to diffusive changes, which occur slowly, and small scale variations in the ambient and track, which occur at relatively faster time scales (smaller spatial scales). Further assume that the diffusive changes are uncorrelated with the small scale changes and occur at distinctly different spatial scales. Then an appropriate choice of the maximum width is not the simple maximum, but rather the maximum of a low pass filtered value of the edge. We therefore perform a low pass filter on the width with a window of 1/2 the track length (typically 50-100 km), then select the maximum of the filtered data for ρ.

Choosing this "filtered maximum" gave reasonable solutions at all ranges for $y_e < \rho$, but introduces a third problem. Namely, the iteration has no solution for $y_e > \rho$. To allow for solutions, we expand on the filtering technique. We define a "standard error" as

$$\alpha = \max(y_e) - \max(y_e') = \rho - \rho'$$

where primes denote the filtered data. Recall that at $x(\rho)$, $\sigma_y = y_e$, so our standard error is also a measure of the variability in the horizontal plume parameter. Next, we add the standard error

to ρ and iterate for σ_y at all ranges. Since ρ is artificially large, a solution is available at all ranges. Finally, we correct the plume parameter by assuming the error in σ_y scales linearly with its magnitude, i.e.,

$$\sigma_y(x,\rho)=\sigma_y(x,\rho+\alpha)+\frac{\alpha}{\rho}\sigma_y(x,\rho+\alpha) \quad x\le x(\rho)$$

$$\sigma_y(x,\rho)=\sigma_y(x,\rho+\alpha)-\frac{\alpha}{\rho}\sigma_y(x,\rho+\alpha) \quad x>x(\rho)$$

where the dependence on ρ is shown explicitly.

This methodology was applied to plume widths measured with a basic edge detection technique. Data were accepted only if the peak cross-track reflectivity was at least twice the standard deviation of the ambient (off-track) reflectivity. This signal-to-noise ratio screening ensured that the edges detected where those of the track rather than ambient spatial structures or broken clouds.

APPENDIX B. CORRELATION STATISTICS

DATE (JUNE 94)	SHIP REPORTS	TOTAL SHIPTRACKS	EXTRACTED SHIPTRACKS	SHIP-SHIPTRACK CORRELATIONS	PERCENT CORRELATED
1	169	8	8	3	37.5
2	322	15	9	3	33.3
3	434	12	7	2	28.6
4	334	11	4	1	25.0
5	201	30	18	1	5.6
6	309	23	11	0	0
7	418	23	5	2	40.0
8	329	38	9	3	33.3
9	415	60	34	15	44.1
10	322	33	26	7	26.9
11	241	60	51	10	19.6
12	241	83	57	25	43.9
13	290	61	39	20	51.3
14	310	71	34	22	64.7
15	427	72	35	11	31.4
16	491	7	2	1	50.0
17	478	20	7	2	28.6
18	389	15	4	3	75.0
19	325	39	12	0	0
20	333	48	34	1	2.9
21	425	25	15	1	6.7
22	399	23	12	2	16.7
23	447	43	16	1	6.3
24	398	40	16	3	18.8
25	401	31	15	1	6.7
26	390	27	12	4	33.3
27	405	115	42	17	40.5
28	338	113	69	15	21.7
29	434	86	53	13	24.5
30	391	130	79	20	25.3
TOTALS	10,806	1362	735	209	28.4

APPENDIX C. SHIP CHARACTERISTICS FOR MAST CORRELATIONS

KEY		
PROPULSION TYPE:		**FUEL TYPE:**
1 FOR OIL BURNING DIESEL ENGINES,		1 FOR HIGH VICOSITY FUEL & DIESEL FUEL,
2 FOR STEAM TURBINE		2 FOR OIL FUEL

SHIP NAME	CALL SIGN AND CORRELATION ID	GROSS TONN-AGE	L (m)	PROP TYPE	POWER RATING (kW)	FUEL TYPE	SPEED CAP. NORMAL WX., LOAD
* TOLUCA	3EFY7.F173.1519	31340	198	1	16241	1	N/A
* NIPPON HIGHWAY	3ENR6.AV178.1753	15546	199	1	12357	1	17.5
HYUNDAI NO 11	3EOB9.UKH.167.0022	14779	157	1	7944	1	16
* KURAMA	3EOF7N163,1336	57870	290	1	40602	1	23.5
* CANADIAN HIGHWAY	3EXH4.AR178.1651	12737	200	1	12357	1	18
* HANJIN BARCELONA	3EXX9.AA181.0046	50792	277	1	37868	1	N/A
* BROOKLYN BRIDGE	3EZJ9.C181.0052	48237	276	1	27529	1	N/A
CENTURY HIGHWAY NO 1	3FFJ4.AT178.1651	43198	186	1	10401	1	18.5
* NEWPORT BRIDGE	3FGH3.K160.1640	48220	277	1	30632	1	N/A
* EVER ROYAL	3FGI3.A161.1618	46875	294	1	30000 est	1	N/A
* HANJIN PORTLAND	3FSB3.AC163.1745	50792	289	1	37868	1	N/A
* SCARLET SUCCESS	3FZI3.S162	17428	N/A	1 est.	8000	1 est.	N/A
* ZIM AMERICA	4XGR.AQ178.1651	37209	236	1	21655	1	21
* ZIM JAPAN	4XGV.M161.1400	37209	236	1	21680	1	21
ZIM SAVANNAH	4XIL.UKH.172.0102	36263	238	1	25892	1	22.5
CALIFORNIA CERES	7JOB.D169.1645	31694	221	1	23023	1	23
* GLOBAL HIGHWAY	7KFY.AS179.1629	19700	200	1	11181	1	18.5
* CENTURY LEADER NO 1	7LHH.AJ180.1438	45422	179	1	9783	1	18
* CENTURY HIGHWAY NO 3	8JNP.AC164.1653	46186	186	1	10549	1	18.5
* CALIFORNIA GALAXY	9VYK.L163.1336	36375	202	1	18537	1	N/A
PRINCE OF TOKYO	A8GJ.X163.1535	34611	194	1	9121	1	14
OOCL FAME	BMEJ.CA181.1546	57366	290	2	59654	2	23
* TAI HE	BOAB.UKH166.1818	35963	236	1	16749	1	N/A
CAPE MAY (WDOU)	WDOU	21667	267	2	26480	2	19.5
BRISBANE STAR	C6LY4.G153.0333	27305	203	1	21324	1	N/A
POLYNESIA	D5NZ.DA154d.1801	10774	162	1	6513	1	16
* HANJIN SAVANNAH	D9MX.BD178.1753	35598	241	1	20853	1	22
* NED LLOYD SINGAPORE	DJNN.U165.1311	14961	170	1	15074	1	N/A
PACKING	ELBX3.AC174.1704	20627	183	1	9599	1	15.5
* PACPRINCE	ELED7.V165.1311	24632	188	1	6988	1	15.3
* OOCL FAIR	ELFV2.AX181.1316	40080	241	1	24362	1	21.5
* OOCL FIDELITY EX.BR.BRG	ELFV8.Q160.1413	40980	241	1	21780	1	21.5
* ALLIGATOR PRIDE	ELJO8.E161.1618	41126	244	1	25083	1	21.6
* ORION	ELJT7.B152.1606	44576	179	1	10710	1	18.5
* CONVEYOR	ELKD.K164.1323	39503	243	2	12137	2	15.5
* OCEAN HIGHWAY	ELKD6.159M1LL3.0020	13857	185	1	12357	1	18.5
SAN MARCOS	ELND4.AD165.1720	15192	190	1	12357	1	19
* GLORIA PEAK	HPPK.AB163.1535	12816	161	1	8496	1	17
CAPE MAY	JBCN.K168.1821	42145	248	1	23750	1	22
GINGA MARU	JFKC.K179.0116	4888	114	1	4560	1	18
* CALIFORNIA MERCURY	JGPN.K160.1413	41442	247	1	21648	1	22
* HENRY HUDSON BRIDGE	JKLS.X176.1818	42407	241	1	21074	1	22.5
* HERCULES HIGHWAY	JKOW.AB164.1653	46875	179	1	8753	1	18.5
* NYK SUNRISE	JPAQ.181.1546.2.M2LL2	43209	252	1	29797	1	23.4
MATSONIA	KHRC.B163.0112	19301	231	2	22067	2	25
TONSINA	KJDG.CC181.1546	60384	264	2	22067	2	17

SHIP NAME	CALL SIGN AND CORRELATION ID	GROSS TONN-AGE	L (m)	PROP TYPE	POWER RATING (kW)	FUEL TYPE	SPEED CAP. NORMAL WX., LOAD
* MANULANI	KNIJ.H163.1336	23785	219	2	23538	2	20
KEYSTONE CANYON	KSFK.H159.1522	81776	260	2	19639	2	15
DIRECT KIWI	LACP4.UKH155.0109.1	20393	189	1	16771	1	20
* SKAUGRAN	LADB2.C161.1400	16366	173	1	10993	1	15
DIRECT KOOKABURRA	LAJI4	27823	227	1	14270	1	18.5
LONDON ENTERPRISE	MQWA5.T158.1543	30479	210	1	11176	1	N/A
MARIE MAERSK	OULL2.I164.0054	52181	294	1	38190	1	N/A
* MAGLEBY MAERSK	OUSH2.J177.1806	52181	294	1	38190	1	24
* ANDERS MAERSK	OXIT2.M3LL2.1846	33401	239	1	33689	1	N/A
* ANNA MAERSK	OXSF2.L172.1541	33400	239	1	33689	1	N/A
* MONTERREY	PGAF.E152.1606	31430	119	1	15745	1	N/A
OAXACA	PGLA.UKH168.1821	31430	198	1	16241	1	18
* JO OAK	PJLS.H158.1543	21541	175	1	11033	1	16
* STAR LIVORNO	S6BO.X180.1608	26171	180	1	9562	1	18
* MERCURY	V7AF.C152.1606	11961	154	1	5884	1	15.5
* OOCL FREEDOM	VRCV.W160.1640	40978	241	1	21927	1	14
OOCL FRONTIER	VRUC6.AA166.1846	57393	289	2	33529	2	N/A
* MOKU PAHU	WBWK.AH163.1745	14554	133	1	10294	1	N/A
* SEA-LAND CONSUMER	WCHF.I163.1336	23763	219	2	23538	2	N/A
* SEA-LAND RELIANCE	WFLH.J161.1618	29965	272	2	23538	2	N/A
* SEA-LAND INDEPENDENCE	WGJC.U162.1348	32629	257	1	22177	1	22.5
* KAIMOKU	WGJT.A156.0057	17525	241	2	22067	2	N/A
* LURLINE	WLVD.BC178.1753	24901	251	2	22067	2	25
* PRESIDENT MONROE	WNRD.R162.1348	40627	262	1	31776	1	25
* R. J. PFEIFFER	WRJP.AT166.1846	31573	204	1	24764	1	N/A
PRESIDENT ADAMS	WRYW.S175.1616	61926	275	1	41897	1	N/A
* MAUI	WSLH.Z163.1535	24544	219	2	23538	2	20

APPENDIX D. COMPOSITE STATISTICS

KEY TO ABBREVIATIONS USED	
Variable	
N	NO. OF DATA POINTS USED IN CALCULATION
TN	SHIPTRACK IDENTIFICATION NUMBER
UT	TRUE WIND SPEED (KTS)
UR	RELATIVE WIND SPEED (KTS)
PT	PROPULSION TYPE 1=DIESEL, 2=STEAM
KW	POWER RATING (kW)
AVVECT3A	N/A, USED FOR OTHER ANALYSIS
SIGYOFMX	N/A, USED FOR OTHER ANALYSIS
MAXDEL3	N/A, USED FOR OTHER ANALYSIS
X_KM	DOWNTRACK DISTANCE (KM)
XNORM	NORMALIZED DOWNTRACK DISTANCE (KM)
A1	LOW 1 AMBIENT REFLECTANCE (%)
A3	LOW 3 AMBIENT REFLECTANCE (%)
MAX1	LOW 1 SHIPTRACK REFLECTANCE (%)
MAX3	LOW 3 SHIPTRACK REFLECTANCE (%)
DPC1	DELTA PERCENT CHANGE LOW 1 (%)
DPC3	DELTA PERCENT CHANGE LOW 3 (%)
WIDTHF	FILTERED SHIPTRACK WIDTH (KM)
SIGYOF	FILTERED SIGMA Y (KM)
NOTE: To get the composite average shiptrack length values, X and Xnorm must be doubled.	

COMPOSITE (131) - JUN94					
Variable	N	Mean	Std Dev	Minimun	Maximum
TN	30144	115.9536226	68.9713014	1	222
UT	30144	15.3784833	5.7553054	3	34
UR	30144	22.0725219	7.9442343	6.4	53.3
PT	30144	1.122147	0.327461	1	2
KW	30144	20368.58	9125.32	5880	40600
AVVECT3A	30023	10.7103181	4.2711475	1.26	25.6
SIGYOFMX	29363	3.2677128	2.1057524	1.15	10.6
MAXDEL3	30144	9.5843292	3.9678789	2.92	24.9
X_KM	30144	147.92778	116.5290926	0	680
XNORM	30144	106.4940278	95.0930645	0	614
A1	23059	35.9268251	12.452396	3.25	99.2
A3	23059	10.9940981	4.2149516	0	30.5
MAX1	30144	35.7704525	13.4916515	2.94	99.8
MAX3	30144	13.9389003	5.3618548	0.45	40
DPC1	23059	6.8496422	26.2552231	-89.8	250
DPC3	23059	36.8394519	33.9792399	-72.2	250
WIDTHF	30144	9.1560539	4.6384737	0	39
SIGYOF	27625	4.4318194	2.4925289	0.314	21.1
COMPOSITE (5) - 29JUN94 - 1608Z					
Variable	N	Mean	Std Dev	Minimun	Maximum
TN	1165	86.2103004	52.8718339	14	175
UT	1165	13.3373391	7.6097032	5	30
UR	1165	21.203691	8.0735416	16.2	42.5
PT	1165	1	0	1	1
KW	1165	19842.76	11706.05	9560	37868
AVVECT3A	1165	14.091588	4.9983023	9.11	21.2
SIGYOFMX	1165	2.6279056	0.5776807	1.45	3.21
MAXDEL3	1165	9.1499571	1.8452293	6.92	12.1
X_KM	1165	145.3064378	108.8180233	0	427
XNORM	1165	77.472806	54.8791504	0	224
A1	851	34.4206816	9.7095136	14.8	53.2
A3	851	14.1876381	5.1632812	4.87	27.3
MAX1	1165	34.997133	10.5954118	9.42	59.6
MAX3	1165	17.0277253	5.8568698	5.4	34.5
DPC1	851	6.0438125	21.3629551	-67.9	104
DPC3	851	28.0802098	26.2247843	-22.5	164
WIDTHF	1165	7.8971073	3.2046223	0	18.8
SIGYOF	1091	3.8756462	1.9661978	1.2	12.8

COMPOSITE (5) - 29-30JUN94 - 14 HRS - HANJIN BARCELONA					
Variable	N	Mean	Std Dev	Minimun	Maximum
TN	1443	15.2674983	1.4573801	13	17
UT	1443	16.9410949	2.8883516	12	20
UR	1443	15.1844075	2.0433138	13	18.4
PT	1443	1	0	1	1
KW	1443	37868	0	37868	37868
AVVECT3A	1443	10.7409425	1.0552584	9.22	12.6
SIGYOFMX	1443	2.0627512	0.9186946	1.17	3.48
MAXDEL3	1443	13.7177408	2.9798219	10.4	17.3
X_KM	1443	162.5398475	111.5016294	0	451
XNORM	1443	186.4654505	139.8842232	0	580
A1	1379	40.5045975	15.3618444	9.99	99.2
A3	1379	10.7248658	2.28775	4.06	21.8
MAX1	1443	41.6026334	18.8281297	5.26	99.8
MAX3	1443	14.864657	3.2211248	8.49	35.7
DPC1	1379	4.4266913	40.1412425	-89.8	850
DPC3	1379	42.1156409	32.1735067	-23.6	369
WIDTHF	1443	10.8472419	4.856086	0	27.5
SIGYOF	1355	5.3982583	3.0569014	1.07	13.6

COMPOSITE (2) - 12JUN94 - 1535Z - WCHF, KNIJ					
Variable	N	Mean	Std Dev	Minimun	Maximum
TN	409	173.8704156	16.9174852	155	189
UT	409	16.5550122	0.4975731	16	17
UR	409	21.3821516	6.1699064	14.5	26.9
PT	409	2	0	2	2
KW	409	23500	0	23500	23500
AVVECT3A	409	14.7215159	0.646845	14	15.3
SIGYOFMX	409	1.9034474	0.1044903	1.81	2.02
MAXDEL3	409	11.6876773	3.1446619	8.18	14.5
X_KM	409	102.9877751	61.2020308	0	226
XNORM	409	84.0733301	51.5171527	0	200
A1	407	43.8174447	3.3017036	32.3	49.1
A3	407	14.7184521	2.6075348	7.97	20
MAX1	409	45.1718826	4.3840024	31.7	52.3
MAX3	409	19.1601467	1.8860429	12.7	26
DPC1	407	3.1197248	6.3179401	-18.2	25.1
DPC3	407	32.9451597	18.5861264	-16.1	126
WIDTHF	409	7.2553545	3.2719271	0	15.1
SIGYOF	357	2.9659384	1.9457991	1.02	8.37

COMPOSITE ALL STEAM TURBINE SHIPTRACKS					
Variable	N	Mean	Std Dev	Minimun	Maximum
TN	3682	169.2593699	35.7718149	114	214
UT	3682	15.7080391	4.0162378	9	24
UR	3682	24.1200163	5.9841817	12.6	41
PT	3682	2	0	2	2
KW	3682	20304.35	4929.59	12100	23500
AVVECT3A	3682	9.8396496	4.2546162	1.26	17
SIGYOFMX	3682	3.7999756	2.2140855	1.57	10.1
MAXDEL3	3682	8.7850869	3.5202936	2.92	18.1
X_KM	3682	127.3780554	92.9780082	0	423
XNORM	3682	81.4186727	57.4240856	0	267
A1	2855	32.9015412	10.0252296	3.25	54.9
A3	2855	10.4502133	4.6009191	0.548	21.2
MAX1	3682	32.968767	11.6118483	2.94	60.6
MAX3	3682	12.8949701	5.2462918	0.45	28.4
DPC1	2855	11.2516009	31.6645521	-68.6	250
DPC3	2855	40.4296865	39.6852221	-72.2	250
WIDTHF	3682	7.999685	3.6808273	0	25.5
SIGYOF	3385	3.9050281	1.8704439	1.02	11.7

COMPOSITE ALL DIESEL SHIPTRACKS					
Variable	N	Mean	Std Dev	Minimun	Maximum
TN	26462	108.5365052	69.2138676	1	222
UT	26462	15.3326279	5.9557982	3	34
UR	26462	21.7876275	8.1391957	6.4	53.3
PT	26462	1	0	1	1
KW	26462	21030.64	9094.22	5880	40600
AVVECT3A	26341	10.8320219	4.259379	1.37	25.6
SIGYOFMX	25681	3.1913999	2.0786632	1.15	10.6
MAXDEL3	26462	9.6955381	4.0136823	2.92	24.9
X_KM	26462	150.7871287	119.159526	0	680
XNORM	26462	109.983086	98.7044992	0	614
A1	20204	36.3543239	12.7004234	3.25	99.2
A3	20204	11.0709537	4.1519043	0	30.5
MAX1	26462	36.1602872	13.6876549	2.94	99.8
MAX3	26462	14.0841558	5.3617505	0.77	40
DPC1	20204	6.2276073	25.3374409	-89.8	250
DPC3	20204	36.3321207	33.0634062	-44.1	250
WIDTHF	26462	9.3169545	4.7341925	0	39
SIGYOF	24240	4.5053833	2.5588494	0.314	21.1

All Ships with HIGH Power Rating (≥ 25,500 kW)					
Variable	N	Mean	Std Dev	Minimun	Maximum
TN	10044	122.760454	76.0008304	9	222
UT	10044	16.1202708	5.2723941	9	34
UR	10044	23.4826563	9.012046	12.6	53.3
PT	10044	1.2196336	0.414019	1	2
KW	10044	30832.34	5536.82	23500	40600
AVVECT3A	10044	10.5278903	2.9091182	5.08	19.2
SIGYOFMX	9776	3.3453897	2.0028355	1.17	10.1
MAXDEL3	10044	9.5107616	3.2513186	2.92	17.3
X_KM	10044	157.2523895	130.1056056	0	680
XNORM	10044	115.8701871	109.4478131	0	614
A1	8352	38.9179358	11.6202679	9.99	99.2
A3	8352	10.8843558	3.4087167	2.82	23.1
MAX1	10044	39.2126394	13.1584367	4.23	99.8
MAX3	10044	14.0558801	4.2207092	1.3	35.7
DPC1	8352	4.7580425	25.5892989	-89.8	850
DPC3	8352	38.0634097	27.9768862	-44.1	369
WIDTHF	10044	9.7668847	4.8562742	0	39
SIGYOF	9273	4.7977733	2.6848906	0.982	17.1
All Ships with MEDIUM Power Rating (> 13,000 kW and < 25,500 kW					
Variable	N	Mean	Std Dev	Minimun	Maximum
TN	10607	131.0719336	68.9978055	1	221
UT	10607	15.5031583	5.7077915	4	30
UR	10607	21.2180824	7.6394276	6.4	43.2
PT	10607	1.0477043	0.21315	1	2
KW	10607	19692.24	2462.21	14300	22200
AVVECT3A	10486	10.6130793	4.4909087	1.26	25.6
SIGYOFMX	10501	3.0400752	2.1474836	1.15	9.76
MAXDEL3	10607	10.4295805	4.6407094	3.25	24.9
X_KM	10607	153.932686	113.2274648	0	546
XNORM	10607	119.0948883	99.9828538	0	495
A1	7594	35.2409784	12.3538904	3.25	71.8
A3	7594	11.2297744	4.5738334	0	30.4
MAX1	10607	34.9442227	13.7839012	2.94	97.8
MAX3	10607	14.0171255	5.6260976	0.45	40
DPC1	7594	9.1475981	34.0558893	-81.1	1100
DPC3	7594	39.2189224	43.625627	-38.7	999
WIDTHF	10607	8.7030329	4.3265391	0	30.8
SIGYOF	9785	3.9718853	2.1968448	0.314	21.1

All Ships with LOW Power Rating (≤ 13,000 kW)					
Variable	N	Mean	Std Dev	Minimun	Maximum
TN	9493	91.8592647	52.8268446	3	213
UT	9493	14.4543348	6.1579116	3	30
UR	9493	21.535247	6.7871818	8	42.5
PT	9493	1.1021806	0.3029016	1	2
KW	9493	10053.19	1562.49	5880	12400
AVVECT3A	9493	11.0107448	5.131379	1.37	24.8
SIGYOFMX	9086	3.4472254	2.1415819	1.38	10.6
MAXDEL3	9493	8.7177257	3.6322968	2.92	21.4
X_KM	9493	131.3523649	102.3699345	0	483
XNORM	9493	82.4940835	63.448235	0	340
A1	7113	33.1469239	12.7474719	3.25	58.9
A3	7113	10.8713426	4.6402688	0.423	30.5
MAX1	9493	33.0516591	12.7223719	2.94	63.2
MAX3	9493	13.7277257	6.0840162	0.78	38.9
DPC1	7113	7.6147713	29.8443252	-81.1	461
DPC3	7113	34.6894175	49.7696631	-72.2	1750
WIDTHF	9493	9.0159518	4.6704271	0	28.8
SIGYOF	8567	4.5610319	2.5132733	1.1	21.1

All **Diesel** Ships with Power Rating > 13,000 kW and < 25,500 kW					
Variable	N	Mean	Std Dev	Minimun	Maximum
TN	10101	127.3366993	68.580647	1	221
UT	10101	15.3068013	5.7512136	4	30
UR	10101	20.5881893	7.2217215	6.4	43.2
PT	10101	1	0	1	1
KW	10101	19571.63	2461.95	14300	22200
AVVECT3A	9980	10.8455772	4.4320015	3.6	25.6
SIGYOFMX	9995	3.0194837	2.1811751	1.15	9.76
MAXDEL3	10101	10.3032017	4.5803562	3.25	24.9
X_KM	10101	156.957925	114.2914968	0	546
XNORM	10101	122.3830769	101.0158264	0	495
A1	7477	35.5042102	12.2174349	3.41	71.8
A3	7477	11.3015779	4.5583451	0	30.4
MAX1	10101	35.7035264	13.4472144	3.49	97.8
MAX3	10101	14.2448797	5.5826308	0.77	40
DPC1	7477	8.4241038	30.6132961	-81.1	1100
DPC3	7477	38.2998511	41.0031084	-38.7	999
WIDTHF	10101	8.8070142	4.3741859	0	30.8
SIGYOF	9318	3.9830487	2.233823	0.314	21.1

All **Steam** Ships with Power Rating > 13,000 kW and < 25,500 kW					
Variable	N	Mean	Std Dev	Minimun	Maximum
TN	506	205.6363636	8.2482631	197	214
UT	506	19.4229249	2.554551	18	24
UR	506	33.7922925	4.0334001	31.1	41
PT	506	2	0	2	2
KW	506	22100	0	22100	22100
AVVECT3A	506	6.0274506	2.9080646	1.26	7.83
SIGYOFMX	506	3.4468182	1.2491947	1.61	5.06
MAXDEL3	506	12.9524111	5.1002452	7.26	18.1
X_KM	506	93.541502	64.550136	0	248
XNORM	506	53.454585	36.4746095	0	140
A1	117	18.4188889	8.9517591	3.25	39.9
A3	117	6.6411026	2.9404502	0.548	13.9
MAX1	506	19.7866601	11.4891532	2.94	60.6
MAX3	506	9.4705929	4.4396362	0.45	28.4
DPC1	117	55.3832137	115.4469633	-61.2	612
DPC3	117	97.9530769	112.6472122	-37	600
WIDTHF	506	6.6273123	2.4354375	0	13.1
SIGYOF	467	3.7491435	1.2282351	1.1	6.33

LIST OF REFERENCES

Albrecht, B.A., 1989: Aerosols, cloud microphysics and fractional cloudiness. *Science*, **245**, 1227-1230.

Brenner, J., 1994: Continental aerosol effects on stratocumulus microphysics during MAST 1994. M.S. Thesis, Naval Postgraduate School, Monterey, CA, 60pp.

Brown, A., 1995: Temporal effects of shiptracks on clouds. M.S. Thesis, Naval Postgraduate School, Monterey, CA, 122pp.

Charlson, R.J., J.E. Lovelock, M.O. Andreae, and S.G. Warren, 1987: Oceanic phytoplankton, atmospheric sulphur, cloud albedo, and climate. *Nature*, **326**, 655-661.

Charlson, R.J., S.E. Schwartz, J.M. Hales, R.D. Cess, J.A. Coakley Jr., J.E. Hansen and D.J. Hofman, 1992: Climate forcing by anthropogenic aerosols. *Science*, **255**, 423-430.

Coakley, J.A. Jr., R.L. Bernstein and P.A. Durkee, 1987: Effect of ship-stack effluents on cloud reflectivity. *Science*, **237**, 1020-1022.

Conover, J.H., 1966: Anomalous Cloud Lines. *J. Atmos. Sci.*, **23**, 778-785.

Durkee, P.A., 1994: *Monterey Area ShipTrack Experiment [CNO Project K-1420] Science Plan.* 42pp.

Gifford, F.A., 1957: Relative atmospheric diffusion of smoke puffs, *J. Met.* **14**, 410-414.

Gifford F.A., 1959: Smoke plumes as quantitative air pollution indices. *Int. J. Air Pollut.* **2**, 42-50.

Gifford, F.A., 1980: Smoke as a Quantitative Atmospheric Diffusion Tracer, *Atmos. Environ.* v14, no.10, 1119-1121.

Gifford, F.A., 1985: Atmospheric diffusion in the range 20-2000km. *Proceedings of the 15th International Technical Meeting on Air Pollution, Modeling and Applications*, St. Louis, MO, 15-19 April, 1985, Plenum Press, New York.

Heffter, J.L. , 1965: The variation of horizontal diffusion parameters with time for travel periods of one hour or longer. *J. Appl. Meteor.*, **4**, 153-156.

71

Hindman, E.E., 1990: Understanding ship-trail clouds. Preprints of 1990 Conference on Cloud Physics, 23-27 July, 1990, San Francisco, CA, A.M.S., Boston, MA.

IPCC (The Intergovernmental Panel on Climate Change), 1994: Radiative Forcing of Climate, World Meteorological Organization and United Nations Environmental Program, in press.

King, M.D., T. Nakajima and L.F. Radke, 1990: Optical properties of marine stratocumulus clouds modified by ship track effluents. Preprints of 1990 Meeting of the American Meteorological Society, San Francisco, CA, 396-400.

Lloyd's, 1992: *Lloyd's Register of Shipping 1992-1993*. Lloyd's Register of Shipping, United Kingdom vol 1-3.

Mays, D., 1993: Shiptrack database analysis. M.S. Thesis, Naval Postgraduate School, Monterey, CA, 65pp.

Mikkelsen, T., 1983: *The Borris Field Experiment: Observations of Smoke Diffusion in the Surface Layer over Homogeneous Terrain*. Risø National Laboratory, Roskilde, Denmark, 61pp.

Mineart, G.M., 1988: Multispectral satellite analysis of marine stratocumulus cloud microphysics. M.S. Thesis, Naval Postgraduate School, Monterey, CA, 138pp.

Nielsen, K.E. and P.A. Durkee, 1992: A robust algorithm for locating ship track cloud features using 3.7 micron satellite data. Preprints to the Papers on the 6th Conference on Satellite Meteorology and Oceanography, 5-10 January, 1992, Atlanta, GA.

ONR (Office of Naval Research), 1994: *Monterey Area ShipTrack Experiment [CNO Project K-1420] Operations Plan*, pp. 1.1 - B12.

Pettigrew, J.C., 1992: Surface meteorological parameters of identified shiptracks. M.S. Thesis, Naval Postgraduate School, Monterey, CA, 72pp.

Porch, W.M., C.J. Kao, and R.G. Kelley, 1990: Ship trails and ship induced cloud dynamics. *Atmos. Environ.,* **24A,** 1051-1059.

Radke, L.F., J.A. Coakley, Jr. and M.D. King, 1989: Direct and remote sensing observations of the effects of ships on clouds. *Science,* **246,** 1146-1149.

Roberts, O.F.T., 1923: The theoretical scattering of smoke in a turbulent atmosphere. *Proc. Roy. Soc.* **A104,** 640-654.

Rogerson, S.D., 1995: Implications of Shiptracks on Ship Surveillance. M.S. Thesis, Naval Postgraduate School, Monterey, CA, 57pp.

Skupniewicz, C.E., and Schacher, G.E., 1986: Parameterization of Plume Dispersion Over Water. *Atmospheric Environment*, 7, 1333-1340.

Skupniewicz, C.E., 1995: Personal communications.

Trehubenko, E.J., 1994: Shiptracks in the Californian Stratus Region: Dependency on Marine Atmospheric Boundary Layer Depth. M.S. thesis, Naval Postgraduatete School, Monterey, CA, 88pp.

Turner, D.B., 1994: *Workbook of Atmospheric Dispersion Estimates, an Introduction to Dispersion Modeling*. CRC Press, Inc., Boca Raton, FL.

Wark, K. and C.F. Warner, 1976: *Air Pollution Its Origin and Control*. Harper and Row Publishers, New York, 519pp.

Zannetti, P., 1990: *Air Pollution Modeling: Theories, Computational Methods and Available Software*. Von Nostrand Reinhold, New York, 444pp.

INITIAL DISTRIBUTION LIST

		No. Copies
1.	Defense Technical Information Center Cameron Station Alexandria, Virginia 22304-6145	2
2.	Library, Code 52 Naval Postgraduate School Monterey, California 93943-5101	2
3.	Chairman (Code MR/Hy) Department of Meteorology Naval Postgraduate School Monterey, California 93943-5002	1
4.	Chairman (Code OC/Bf) Department of Oceanography Naval Postgraduate School Monterey, California 93943-5002	1
5.	Professor Philip Durkee (Code MR/De) Department of Meteorology Naval Postgraduate School Monterey, California 93943-5002	1
6.	Professor Carlyle H. Wash (Code MR/Wx) Department of Meteorology Naval Postgraduate School Monterey, California 93943-5002	1
7.	Mr. Bob Bluth Office of Naval Research Code 4513 Room 522 800 North Quincy St. Arlington, Virginia 22217-5000	1
8.	Dr. David Johnson Office of Naval Research Code 1243 Room 522 800 North Quincy St. Arlington, Virginia 22217-5000	1

9. Oceanographer of the Navy   1
   Naval Observatory
   34th and Massachusetts Avenue NW
   Washington, DC 20390-5000

10. Commander   1
    Naval Meteorology and Oceanography Command
    Stennis Space Center, Mississippi 39529-5000

11. Chief of Naval Research   1
    800 North Quincy Street
    Arlington, Virginia 22217

12. Commanding Officer   1
    Fleet Numerical Meteorology and Oceanography Center
    Monterey, California 93943

13. LT Raymond E. Chartier Jr.   2
    142 Brownell Circle
    Monterey, California 93940